Key Points:
- Seamless distributed parameter maps can be obtained for the gridded hydrologic model wflow_sbm with transfer functions from literature
- Application of wflow_sbm with these seamless parameter maps yields simulation results with high KGE and NSE across the Rhine basin
- Fluxes matched across model scales for evapotranspiration, but this match was considerably less for fluxes affected by (sub)surface flows

Correspondence to:
R. O. Imhoff,
Ruben.Imhoff@deltares.nl

Scaling Point-Scale (Pedo)transfer Functions to Seamless Large-Domain Parameter Estimates for High-Resolution Distributed Hydrologic Modeling: An Example for the Rhine River

R. O. Imhoff[1,2] , **W. J. van Verseveld[3]** , **B. van Osnabrugge[1,2]** , and **A. H. Weerts[1,2]**

[1]Operational Water Management, Department of Inland Water Systems, Deltares, The Netherlands, [2]Hydrology and Quantitative Water Management Group, Wageningen University & Research, Wageningen, The Netherlands, [3]Catchment and Urban Hydrology, Department of Inland Water Systems, Deltares, The Netherlands

Abstract Moving toward high-resolution gridded hydrologic models asks for novel parametrization approaches. A high-resolution conceptual hydrologic model (wflow_sbm) was parameterized for the Rhine basin in Europe based on point-scale (pedo)transfer functions, without further calibration of effective model parameters on discharge. Parameters were estimated on the data resolution, followed by upscaling of parameter fields to the model resolution. The method was tested using a 6-hourly time step at four model resolutions (1.2, 2.4, 3.6, and 4.8 km), followed by a validation with discharge observations and a comparison with actual evapotranspiration (ET_{act}) estimates from an independent model (DMET Land Surface Analysis Satellite Application Facility). Additionally, the scalability of parameter fields and simulated fluxes was tested. Validation of simulated discharges yielded Kling-Gupta Efficiency (KGE) values ranging from 0.6 to 0.9, except for the Alps where a volume bias caused lower performance. Catchment-averaged temporal ET_{act} dynamics were comparable with independent ET estimates (KGE ≈ 0.7), although wflow_sbm model simulations were on average 115 mm yr^{-1} higher. Spatially, the two models were less in agreement (SPAEF = 0.10), especially around the Rhine valley. Consistent parameter fields were obtained, and by running the model at the different resolutions, preserved ET_{act} fluxes were found across the scales. For recharge, fluxes were less consistent with relative errors around 30% for regions with high drainage densities. However, catchment-averaged fluxes were better preserved. Routed discharge in headwaters was not consistent across scales, although simulations for the main Rhine River were. Better processing (scale independent) of the river and drainage network may overcome this issue.

Plain Language Summary Hydrologic models are used for flood and drought predictions. Most models have parameters, and to increase model performance, hydrologists often tune these parameters by calibration. State-of-the-art gridded hydrologic models have parameter sets per grid cell, leading to many parameters and making current calibration procedures far from ideal. Here, we tested the use of well-known (pedo)transfer functions from literature to estimate these parameter values, something which can reduce the calibration burden. By using parameter-specific upscaling rules to derive seamless parameter maps for the wflow_sbm model, which explicitly takes subsurface lateral flows into account, this gives a model which is scalable to different grid cell sizes. We assessed the approach on multiple model resolutions, and we found consistent parameter fields and the preservation of vertical fluxes. Only routed discharge, a key output, deteriorates for headwater catchments on coarser resolutions. We attribute this to model structure and the derivation procedure of the river network on different scales, resulting in the loss of lateral flow representation on coarser resolutions. Nevertheless, discharge and evapotranspiration simulations are similar to observations and other models. Hence, regionalization with literature transfer functions and upscaling techniques can further lower the calibration burden and enable predictions in ungauged basins.

1. Introduction

In the European Rhine river, higher winter discharges are expected as a result of climate change (Görgen et al., 2010; Hurkmans et al., 2010; Krysanova et al., 2017; Middelkoop et al., 2001). For both policy and

climate change impact studies (e.g., Te Linde et al., 2010; Photiadou et al., 2011; Wit & Buishand, 2007) and for operational flood forecasting (Reggiani & Weerts, 2008; Renner et al., 2009; Verkade et al., 2017) by the Dutch Ministry of Infrastructure and Water Management, the hydrologic behavior of the Rhine is currently modeled with a semidistributed HBV96 model (Lindström et al., 1997). Model selection and development originate from the late 1990s, following the extreme high water events in 1993 and 1995.

Currently, a transition takes place from lumped to distributed hydrologic models for operational and policy purposes. Within the context of the ongoing H2020 project IMPREX (Van Den Hurk et al., 2016), we aim to improve the physical realism of the hydrologic model and process descriptions for the Rhine, to obtain more trust in the outcomes of such a model. A transition from lumped to gridded models enables the model developer to take advantage of present-day availability of spatial data (for model building, forcing, or constraining). High-resolution spatial data enable the modeler to represent land use and vegetation (e.g., Leaf Area Index (LAI)), as they are observed from space, in spatially distributed hydrologic models. For example, estimates of (shortwave downward) radiation fluxes from geostationary satellites make it possible to estimate potential evapotranspiration at high spatial and temporal resolution (De Bruin et al., 2016). Moreover, high-resolution satellite data provide new ways to test and possibly constrain model simulations, particularly the spatial pattern and magnitude of snow, overland flow, soil moisture, and actual evapotranspiration.

As such, it is clear that a new generation of dynamic and spatially explicit hydrologic models should take advantage of present-day availability of high-resolution spatial data sources. However, the step toward a distributed hydrologic model that takes into account the natural spatial variability within catchments does not automatically lead to more physical realism. Within the ongoing scientific debate, three main topics can be identified: (1) the importance of and link between temporal and spatial scales (see Clark et al., 2017; Melsen et al., 2016, and references therein), (2) model structure and in particular process representation of these spatially distributed models (Clark et al., 2017, and reference therein), and (3) deriving/estimating model parameters for these models (Archfield et al., 2015; Beven, 2006; Bierkens, 2015; Clark et al., 2016; Mizukami et al., 2017; Paniconi & Putti, 2015; Samaniego et al., 2010). Within the bottom-up modeling approach, it is generally believed that if we solve physical hydrologic processes at the right scale and if linked to correct landscape indicators, less (or no further) calibration will be needed. Moving to a distributed model, which resolves relevant processes on high resolution, has consequences and comes at a prize regarding parameter estimations (Archfield et al., 2015; Bierkens, 2015; Beven, 2006; Clark et al., 2016; Mizukami et al., 2017; Paniconi & Putti, 2015; Samaniego et al., 2010).

In Samaniego et al. (2017), an overview is given of the state-of-the-art regarding parametrization and regionalization techniques. They propose the Multiscale Parameter Regionalization (MPR) technique (Samaniego et al., 2010) as a suitable and practical way to obtain seamless parameters across scales. A fundamental step in MPR is the selection of regionalization functions and scaling operators to ensure the transferability of global parameters across spatial scales and to guarantee the seamlessness of parameter fields. A systematic approach of determining these functions is in its infancy, and a generalized approach for determining the scaling operators is not yet available. In the MPR methodology, many transfer function coefficients need to be estimated by calibration (~53 for the mHM model; see Rakovec et al., 2016). These so-called global parameters include the coefficients of the transfer functions that link soil and vegetation properties, such as LAI, sand, and clay content, to physical or model properties (e.g., residual water content and saturated hydraulic conductivity).

To lower the number of calibrated global parameters in the MPR methodology, or minimize calibration, one could use (pedo)transfer functions (PTFs) from literature instead of calibrated relations (for an overview of PTFs developed by the pedometric community; see Van Looy et al., 2017). A large advantage of such an approach is that the transfer functions are not constrained to the model but to actual field measurements. Note that those PTFs are point-scale relationships and that the scale at which these functions can be used remains an issue (Samaniego et al., 2017; Van Looy et al., 2017). However, the availability of high-resolution soil data (e.g., 250 m by Hengl et al., 2017) in combination with the right selection of regionalization functions and scaling operators, ensuring flux preservation on different scales, makes it worthwhile to investigate if point-scale PTFs can be used for hydrologic modeling. This, by using the philosophy of MPR, first derives model parameters on the highest available resolution of the data, followed by scaling to the desired model resolution.

Therefore, the objective of this study is to investigate the applicability of point-scale PTFs in combination with suitable upscaling operators for deriving seamless hydrologic model parameters and the preservation of fluxes across scales for a multiscale hydrologic model for the Rhine River. Within the scope of this study, we try not to implement any further calibration on top of the implementation of the PTFs in order to focus on the model processes. A calibration procedure would limit this, as the results get influenced by parameters constrained to both the observed discharge and the used forcing.

To test the applicability of point-scale PTFs, we use the spatially distributed hydrologic model wflow_sbm. In this model, the soil part is largely based on topog_sbm (Vertessy & Elsenbeer, 1999), and it uses a kinematic wave approach for channel, overland, and lateral subsurface flow routing similar to TOPKAPI (Benning, 1994; Todini & Ciarapica, 2002) and G2G (Bell et al., 2007). The evaluation is based on the following sub-questions: (1) Which PTFs used in wflow_sbm cover the sensitive parameters of this model? (2) What is the quality of the resulting wflow_sbm model on the highest resolution of interest (1,200 m)? (3) How scale (in)dependent are the resulting wflow_sbm modeled fluxes? Note that to the authors' knowledge, the upscaling methodology advocated in MPR was so far only tested using models without subsurface lateral exchange.

This paper is set up as follows: in section 2, the data and study area of this study are presented. Section 3 describes the used methodology, in section 3.1 a description of the wflow_sbm model and parametrization, and in section 3.2 a description of the experimental setup of this study. The results are presented in section 4, followed by the discussion and conclusions in, respectively, sections 5 and 6.

2. Study Area and Data
2.1. Study Area
The studied basin is the Rhine basin upstream of the Dutch border, which has a surface area of approximately 160,000 km^2 (Figure 1). In this figure, we have indicated three subbasins of the Rhine, which are used for the sensitivity analysis and later on to highlight some results. The subbasins are Obsi (748 km^2), part of the Sieg catchment; Elsenz (539 km^2), part of the Neckar catchment; and Omos 2 (2,912 km^2), which is part of the Moselle catchment. These three are all headwaters and located in different regions of the Rhine basin. As such, they are a sample out of the variety of, for example, discharge regimes, soil types, local climates, vegetation properties, and slopes in the Rhine basin.

2.2. Available Data
In this section, we introduce the most important data sets used in the study. A complete list of all data sets can be found in Table A1.
2.2.1. Forcing
A meteorological forcing data set is available for the Rhine basin, consisting of gauged precipitation interpolated with the genRE method (Van Osnabrugge et al., 2017), potential evapotranspiration, and temperature data (Van Osnabrugge et al., 2019), on a 1,200 m grid. Since not all meteorological stations were continuously delivering high-quality data, we refer to Van Osnabrugge et al. (2017, 2019) for an indication of the yearly availability and quality of the forcing data. These forcing data sets are available for the period 1996 through 2015.
2.2.2. DMET LSA SAF Evapotranspiration
For the comparison of simulated actual evapotranspiration (hereinafter referred to as ET_{act}) with model simulations from a land-surface model, the DMET product is used from the Land Surface Analysis Satellite Application Facility (LSA SAF) (Trigo et al., 2011). These data are available from 2011 and onward.

LSA SAF DMET (from hereon referred to as DMET) is a product with daily ET_{act} estimates for terrestrial surfaces and inland water systems, following from physically based Soil Vegetation Atmosphere Transfer models, notably a modified version of the Tiled ECMWF Surface Scheme for Exchange Processes over Land (TESSEL and H-TESSEL; Albergel et al., 2012; Balsamo et al., 2009; Van den Hurk et al., 2000; Viterbo & Beljaars, 1995). The daily values are an integration over instantaneous 30 min ET_{act} estimates. In their approach, Trigo et al. (2011) combine radiative data from the Meteosat Second Generation geostationary satellites with ECMWF meteorological forecasts and land cover information as input for these physically based land surface models (Step 1). DMET then uses tiles within grid cells with a mixture of plant functional types. For each tile, the Soil Vegetation Atmosphere Transfer model solves the surface energy balance and the resulting ET_{act} value per grid cell is then a weighted contribution of all tiles in that cell (Step 2). Finally, a postprocessing module is used to create the daily product (Step 3).
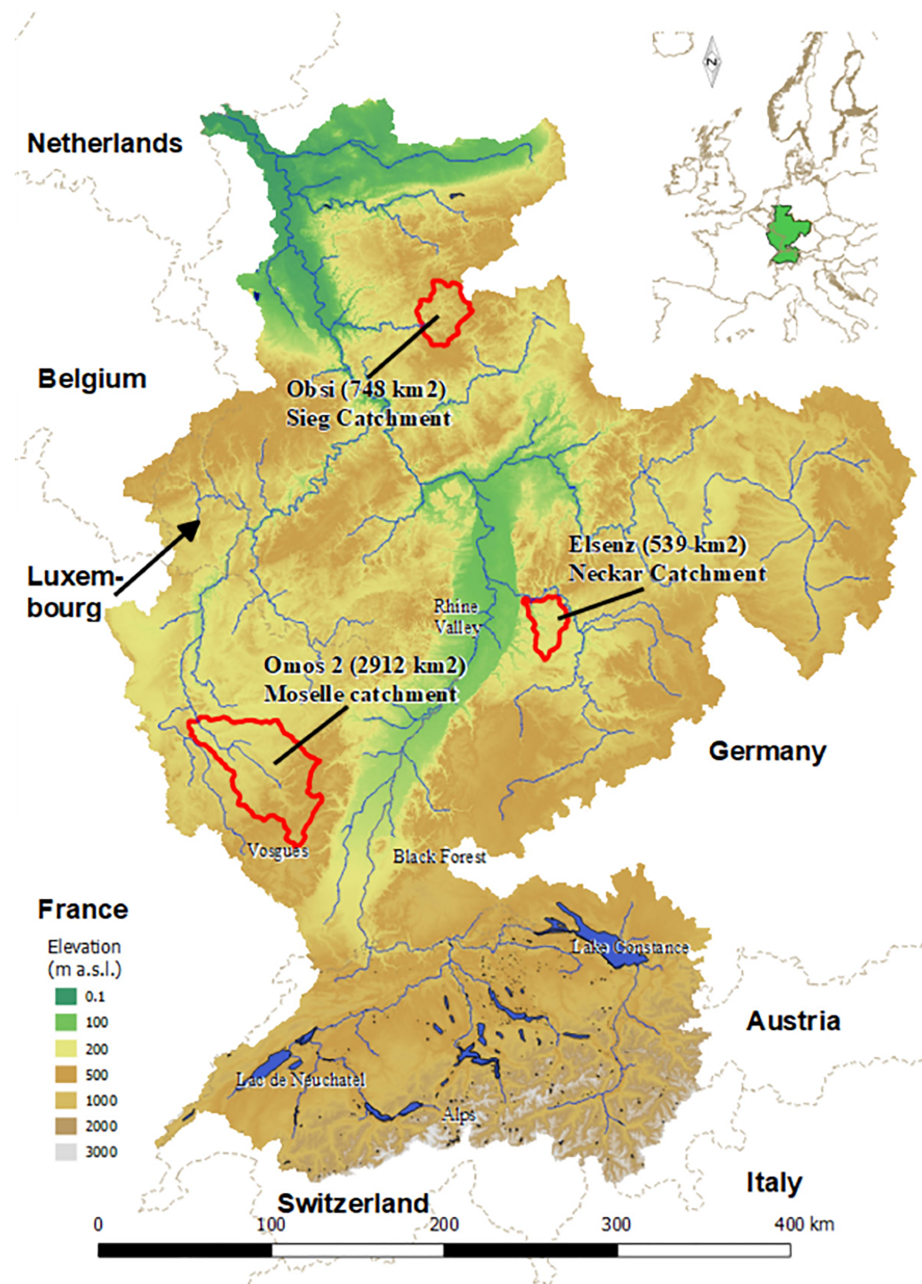
Figure 1. Elevation map, based on the STRM digital elevation model (Farr et al., 2007) and overview of the Rhine basin with three chosen subbasins as study area (in red).

2.2.3. Grid Cell Resolution of the Original Data

The grid cell sizes of the used data sets differ. Whereas it is 1,200 m for model and forcing, it is 3,000 m for DMET, 250 m for soil data of ISRIC SoilGrids (Hengl et al., 2017), 500 m for monthly averages of LAI (Myneni et al., 2015), and 100 m for the CORINE land cover (European Environment Agency, 2018). Topographic characteristics are based on a 30 m rescaling of the SRTM digital elevation model (Farr et al., 2007). The highest spatial resolution determines the base resolution before upscaling, also referred to as "Level 0" in the MPR framework (Samaniego et al., 2010). The handling of the resolution differences between the model resolution and the soil and vegetation properties (the upscaling step), as used for the parameter transfer functions, is described in section 3.1.2. For the comparison between DMET product and the wflow_sbm results, model simulations are upscaled to the DMET resolution following an arithmetic mean.

3. Methodologies

In this section, we briefly introduce the wflow_sbm model (section 3.1), its model setup (section 3.1.1), and parameterization (section 3.1.2), followed by a description of the experimental setup (section 3.2). The experimental setup is subdivided in three sections describing in order the parameter sensitivity analysis (section 3.2.1), the validation of the model setup on the highest model resolution (section 3.2.2), and the scalability of the model (section 3.2.3).

3.1. The wflow_sbm Concept and Modeling Setup

The conceptual bucket model wflow_sbm (Figure 2) is based on topog_sbm (Vertessy & Elsenbeer, 1999) with a kinematic wave approach for lateral subsurface and overland and river flow processes that are similar to TOPKAPI (Benning, 1994; Todini & Ciarapica, 2002) and G2G (Bell et al., 2007). It is available in the wflow open source modeling framework (Schellekens et al., 2020), which is based on PCRaster (Karssenberg et al., 2010) and python. In contrast to many conceptual models, wflow_sbm models lateral subsurface flows explicitly and it has a simplified physical basis with parameters that represent physical characteristics, leading to (theoretically) an easy linkage of the parameters to actual physical properties (Vertessy & Elsenbeer, 1999). While topog_sbm performs best when simulating fast runoff processes in small catchments (Vertessy & Elsenbeer, 1999), wflow_sbm can be applied on a wider variety of catchments (Schellekens et al., 2020). Notable properties of the wflow_sbm model are as follows:

1. A spatially distributed gridded cell network with the presence of lateral subsurface flow based on a D8-network flow routing network (Karssenberg et al., 2010). Flow routing takes place with a kinematic wave module for river, surface, and subsurface lateral flow (comparable to Bell et al., 2007; Todini & Ciarapica, 2002).
2. Parameters that represent environmental physical characteristics such as vegetation and soil properties.
3. A soil divided in saturated and unsaturated store(s). The transfer of water from unsaturated to (un)saturated zones is simulated with the Brooks-Corey equation for the hydraulic conductivity as a function of normalized volumetric water content (Brooks & Corey, 1964).
4. Evapotranspiration and interception losses. The latter via an analytical Gash model on daily time steps or a modified Rutter model on subdaily time steps (Gash, 1979; Rutter et al., 1971; 1975).
5. Capillary rise to the unsaturated store.
6. The option to divide the soil depth in any number of layers instead of one soil column.
7. Reduction coefficients for ET_{act} from the unsaturated zone based on the Feddes curve (Feddes et al., 1978).
8. Glacier buildup and melting processes.

3.1.1. Model Setup

Since a meteorological forcing on a cell size of 1.44 km^2 ($1,200 \times 1,200$ m) is available for this study (see section 2), the same spatial resolution is used as the highest resolution for model runs (Level 1). The model setup in this study has four soil layers: 0–10, 10–40, 40–120, and 120 cm up to the depth of an impermeable layer or bedrock. The first layer, 0–10 cm, is comparable to the depth remotely sensed soil moisture data that are thought to represent (e.g., Dorigo et al., 2017), which should enable spatial comparisons with soil moisture products. The next layer (10–40 cm) represents a layer, dense in plant roots, which reacts rapidly to changes in the meteorological forcing. The layer 40–120 cm represents the depth up to the average end of the soil profile for shallow soils. Below this last layer, wflow_sbm computes a variable depth per grid cell, that is, the layer depth is limited to the maximum soil depth that is set for that grid cell. In this study, we base this depth on the occurrence of an impermeable layer or the presence of bedrock. This is in the current setup never deeper than 2 m, because of data set limitations (ESDAC, 2004; Hengl et al., 2017).

The model is run on a 6-hourly time step. A brief sensitivity analysis (not shown) revealed that at time steps of more than 6 hr, a deterioration of the model results will start, while at a 6-hourly time step and smaller, model results were more or less comparable. An hourly time step is possible with the available meteorological forcing, but coarser temporal resolutions are favorable to decrease run times, especially on the scale of the Rhine basin.

The Rhine basin consists of several large lakes and reservoirs in the Alpine regions. The largest lakes in Switzerland are represented in the model by a lake module, which is also used in other hydrologic models within the wflow framework (Lindström et al., 1997; Schellekens et al., 2020; Van Osnabrugge et al., 2017). This module requires the reservoir locations, their surface areas, initial water levels, and lake operation
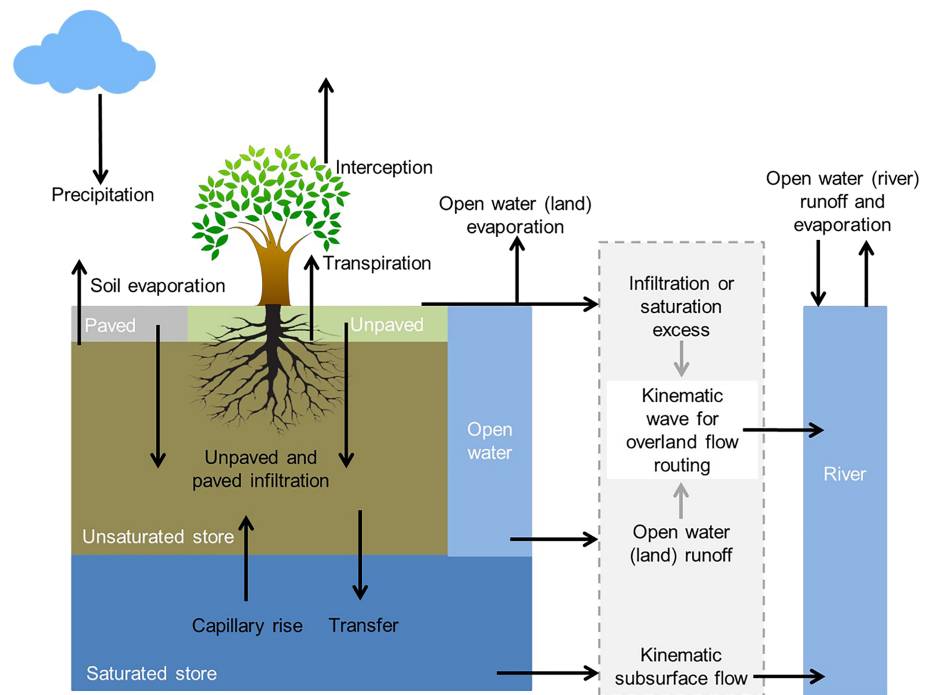
Figure 2. An overview of the processes and fluxes represented by the spatially distributed wflow_sbm model (Schellekens et al., 2020).

schemes, which are available from the operational model used for hydrologic forecasting at the Dutch water authority Rijkswaterstaat.

In addition, Alpine glaciers are modeled on all four resolutions. To do this in wflow_sbm, the initial fraction per grid cell covered by a glacier and the initial storage in these glaciers (in mm) needs to be estimated. The global RGI (RGI Consortium, 2017), GLIMS (Raup et al., 2007), and Swiss GLAMOS (Fischer et al., 2014) databases are used for this, together with glacier volume estimations from Grinsted (2013). The modeling of glaciers introduces three extra parameters in the model, notably:

1. G_SIfrac, the fraction of the snow pack on top of the glacier which is converted into ice per time step. This parameter is set to 0.002 (typically ranges from 0.001 to 0.006 Luo et al., 2013).
2. G_TT, threshold temperature at which precipitation falls as snow on the glacier. Set to 1.3 °C (Tobin et al., 2013).
3. G_fmax, the melting factor (mm·$°C^{-1}$·day^{-1}). Variable from glacier to glacier but set to 5.3 mm·$°C^{-1}$·day^{-1} here based on reported values by Hock (2003).

3.1.2. Parametrization and Upscaling Rules

Model parameters are estimated with available point-scale PTFs from literature (Table 1), leading to seamless parameter maps for these parameters over the entire Rhine basin. Following the MPR methodology, we have estimated the parameters on the original data resolution (often referred to as "Level 0"), followed by upscaling procedures to upscale the parameters to the model resolutions ("Level 1"). These procedures should enable us to use the derived parameter sets on every desired model resolution (Kumar, Samaniego, et al., 2013; Samaniego et al., 2010, 2017).

Universal scaling rules for hydrologic model parameters are not available yet, as they also depend on model structure (Nijzink et al., 2016). However, the right procedure is found when parameter fields remain seamless with a constant mean and standard deviation on various spatial resolutions. The same holds for resulting fluxes and states on various spatial resolutions. That this is possible with the MPR approach was already illustrated for the mHM-model (Kumar, Samaniego, et al., 2013; Samaniego et al., 2010, 2017).

Here, we follow some of the upscaling procedures as used by Zhu and Mohanty (2002), Samaniego et al. (2010), Kumar, Samaniego, et al. (2013), Mizukami et al. (2017), and Samaniego et al. (2017) to estimate parameter values on four model resolutions: 1,200, 2,400, 3,600, and 4,800 m. Generally, these studies slightly

Table 1
List of Parameters Estimated With a PTF and the Used Upscaling Operators

Parameter	Pedotransfer function by	Upscaling operator	Additional notes
c	Rawls and Brakensiek (1989)	log A	λ upscaled with log A, c determined from λ at model resolution
Kext	Van Dijk and Bruijnzeel (2001)	A	Lookup table from land cover
KsatVer	Brakensiek et al. (1984)	log A	
LAI	Myneni et al. (2015)	A	
M			Derived as exponential decay function from KsatVer at seven depths
N	Engman (1986) and Kilgore (1997)	A	Lookup table from land cover
N_River	Liu et al. (2005)		Derived at model resolution, depends on Strahler order
RootingDepth	Fan et al. (2016) and Schenk and Jackson (2002)	A	d_{75} rooting depth
Sl	Pitman (1989) and Liu (1998)	A	Lookup table from land cover
Slope	Farr et al. (2007)	A	PCRaster functionality (Karssenberg et al., 2010), based on DEM
SoilThickness	Hengl et al. (2017) and ESDAC (2004)	A	
Swood	Pitman (1989) and Liu (1998)	A	Lookup table from land cover
thetaR	Tóth et al. (2015)	A	
thetaS	Tóth et al. (2015)	A	

Note. Only the abbreviated parameter names are illustrated; see Table 2 for the interpretation of the parameters. Upscaling operators are abbreviated as follows: A, arithmetic mean and log; A, arithmetic mean of the natural logarithm.

differ in the applied upscaling operators, resulting from differences in the model structures and the types of parameters. The used PTFs and upscaling operators per parameter are listed in Table 1. The equations of the transfer functions are shown in Table B1, and a more detailed description of the parameter estimations is present in the supporting information (Text S1 and Tables S1–S3).

In the approach taken here, no further calibration on observations (e.g., discharge) was applied. Note, however, that for two model parameters, notably the lateral/horizontal hydraulic conductivity and the day-degree parameter for snow and the glaciers, no suitable PTF is available yet. We applied a constant factor (KsatHorFrac) of 250 on the derived vertical hydraulic conductivity at different scales and 1.3 °C for the day-degree (*TT* and G_TT) parameters. The sensitivity of the model results on this choice is discussed in sections 4 and 5.

3.2. Experimental Setup
3.2.1. Parameter Sensitivity Analysis
Table 2 lists all used parameters of the wflow_sbm model. A sensitivity analysis is performed to assess which of the wflow_sbm parameters have a pronounced influence on both discharge and ET_{act} simulations. With the outcomes, we can determine if all sensitive parameters are estimated with a tranfer function, while the less sensitive parameters can be set to a default value in the absence of a PTF. The sensitivity analysis is applied on three subbasins (Figure 1), which are chosen based on their variety in soil type, geographical location, and catchment size to have a representation of the catchment variety within the Rhine basin.

A Latin Hypercube One-factor-At-a-Time sensitivity analysis is applied for the period 1 October 2014 until 1 January 2016 with $N = 100$ LH points. Hence, 100×23 (number of used parameters + 1 reference) model runs are necessary for this sensitivity analysis. The Latin Hypercube One-factor-At-a-Time analysis uses loops with each loop having one of the LH points. Each LH point j then has a partial effect ($S_{i,j}$) for each

Table 2
wflow_sbm Parameters That Are Part of the Sensitivity Analysis

Parameter name	Parameter interpretation	Lowest value in range	Highest value in range	PTF
Soil parameters				
c	Exponent in the Brooks-Corey equation to calculate the hydraulic conductivity as a function of normalized volumetric water content (-). This equation is used to simulate the transfer of water from unsaturated to (un)saturated zones.	1.0	20	✓
KsatHorFrac	A multiplication factor applied to the KsatVer parameter that gives the horizontal saturated conductivity of the soil at the surface (-).	0.1	10,000	
KsatVer	Vertical saturated conductivity of the soil at the surface (mm day^{-1}).	1.0	10,000	✓
M	Decay of KsatVer with depth (-).	1.0	3,000	✓
SoilThickness	Depth of the upper aquifer (mm).	100	5,000	✓
thetaR	Residual water content (-).	0.01	0.25	✓
thetaS	Saturated water content (-).	0.25	0.95	✓
Transpiration				
CapScale	Scaling factor in the capillary rise calculations (-).	0.50	1.50	
rootdistpar	Curvature value for root connection with the groundwater table (mm).	−0.01	−10,000	
RootingDepth	Length of the vegetation roots [mm].	100	5,000	✓
Interception				
Kext	Extinction coefficient in the canopy gap fraction equation [-].	0.48	0.96	✓
Sl	Specific leaf storage (mm).	0.02	0.2	✓
Swood	The fraction of wood in the vegetation/plant (-).	0.0	0.5	✓
Flux partitioning				
InfiltCapPath	Infiltration capacity of the compacted soil/paved (mm day^{-1}).	5.0	500	
InfiltCapSoil	Infiltration capacity of the non-compacted soil (mm day^{-1}).	10.0	2,500	
MaxLeakage	Maximum leakage (mm day^{-1}).	0.0	2.0	
PathFrac	Fraction of compacted or urban area per grid cell (-).	0.0	0.2	✓
Routing				
N	Manning's roughness coefficient for overland flow (m$^{-\frac{1}{3}}$ s).	0.008	0.96	✓
N_River	Manning's roughness coefficient for river flow (m$^{-\frac{1}{3}}$ s).	0.003	0.7	✓
Snow				
TT	Threshold temperature at which precipitation falls as snow (HBV parameter) [°C].	−2.0	2.0	
TTI	Critical snowmelt and refreezing temperature (HBV parameter) (°C).	0.0	3.0	
WHC	Fraction of water stored in snow volume (HBV parameter) (-).	0.01	0.3	

Note. The right column indicates whether these parameters have a PTF or not. Also, the parameter value ranges for the sensitivity analysis are displayed.

parameter e_i (Van Griensven et al., 2006):

$$S_{i,j} = \frac{100 \cdot \left(\frac{g \cdot a - g \cdot b}{[g \cdot a + g \cdot b]/2}\right)}{f_i}$$
$$a = (e_1, \ldots, e_i \cdot (1 + f_i), \ldots, e_p)$$
$$b = (e_1, \ldots, e_i, \ldots, e_p)$$

(1)

In these equations, g refers to the model functions and f_i is the fraction by which parameter e_i is changed (Van Griensven et al., 2006). This fraction is 0.02 in this study. The partial effect is determined for model simulations of discharge and $\mathrm{ET_{act}}$. Finally, the mean partial effect per parameter is ranked to give an indication of the relative parameter sensitivity.

3.2.2. Validation of the wflow_sbm Model for the Rhine
The model is run for the Rhine basin for the period 1 January 1998 until 31 December 2015, with the first year as warm-up period. In the following paragraphs, the model setup validation for this model run is described.

3.2.2.1. Discharge Validation on the Highest Resolution
Validation of simulated discharge on 1,200 m takes place by a comparison with discharge observations at 174 gauging stations. The metrics Kling-Gupta Efficiency (KGE) and Nash-Sutcliffe Efficiency (NSE) are used for this (Gupta et al., 2009; Nash & Sutcliffe, 1970).

Moreover, the lakes in Switzerland and Southern Germany have a pronounced effect on the behavior of the Alpine basins and the main course of the Rhine River. The lake operation procedures of the eight largest lakes are also modeled in this study. Therefore, the simulated lake levels of these eight lakes are validated with observed lake levels.

3.2.2.2. Validation of Evapotranspiration Estimates
Current practice to assess model performance is often to solely use discharge observations as a means for the overall performance. Since we are dealing with a gridded hydrologic model, spatial model outputs can also be assessed for model performance. Here, we focus next to discharge on simulated $\mathrm{ET_{act}}$ (as is also done in, e.g., Kunnath-Poovakka et al., 2016; Stisen et al., 2011; Wanders et al., 2014). For the assessment of $\mathrm{ET_{act}}$, Demirel et al. (2018) and Koch et al. (2018) have introduced a new efficiency metric, the Spatial Efficiency Metric (SPAEF), which resembles the KGE in that it equally weighs multiple components. It is formulated as follows:

$$SPAEF = 1 - \sqrt{(\phi - 1)^2 + (\chi - 1)^2 + (\psi - 1)^2}, \tag{2}$$

with

$$\phi = \rho(A, B), \tag{3}$$

$$\chi = \frac{\left(\frac{\sigma_A}{\mu_A}\right)}{\left(\frac{\sigma_B}{\mu_B}\right)}, \tag{4}$$

$$\psi = \frac{\sum_{j=1}^{n} min(K_j, L_j)}{\sum_{j=1}^{n} K_j}. \tag{5}$$

In these equations, ϕ is the Pearson correlation coefficient between "observed" and simulated $\mathrm{ET_{act}}$, χ is the fraction of coefficient of variations, which represents the spatial variability, and ψ is the percentage of histogram intersection between observations and simulations, with K the histogram of the DMET simulations and L the histogram of the model simulations with n bins. The difference from other spatial metrics is especially pronounced in ψ, because this term is sensitive to clusters in spatial patterns (Demirel et al., 2018; Koch et al., 2018). Hence, this assures that the efficiency metric performs not only on the pixel scale but also on a larger scale. This is a useful addition, as the model is compared with another model, and "observed" pixel values are not per definition the true values.

We assess modeled $\mathrm{ET_{act}}$ with the estimations from DMET by means of the attained SPAEF as a measure for the spatial validation of temporally averaged $\mathrm{ET_{act}}$ fluxes. The KGE is used for a temporal assessment of subbasin-averaged daily $\mathrm{ET_{act}}$ simulations.

3.2.2.3. Validation of Snow Water Equivalent Estimates

Validation of simulated snow water equivalent (SWE) takes place by a comparison with modeled SWE from SLF (Jörg-Hess et al., 2014). SLF simulations are available for the same period as the model runs and for all Swiss basins on a subbasin level (~1,000 km^2) and a weekly temporal resolution. The results of this validation are not shown here but are available in Figures S13–S15 of the supporting information.

3.2.3. Scalability of the Model

To evaluate the outcomes of the parameter estimation and upscaling procedures, we have used the obtained parameter maps and the results from the model runs to assess whether parameter maps, states, and fluxes remain constant on different resolutions. First, mean values and standard deviations in parameter maps are compared to show how the parameters are influenced by spatial scaling.

Second, the relative error in modeled fluxes and states is compared to those on the highest model resolution (1,200 m). This cross-spatial comparison of modeled fluxes is also called flux matching and is used as a measure of the scale insensitivity of MPR-based hydrologic models (e.g., Kumar, Samaniego, et al., 2013; Samaniego et al., 2017).

Third, the performance of the model across the different scales is investigated by comparing the KGE for simulated discharge on the four resolutions with observations. For this, 19 (of the 174) gauging stations across the Rhine basin are used.

4. Results

4.1. Parameter Sensitivity Analysis

The top five most sensitive parameters per subcatchment and per efficiency metric are colored blue in Table 3. The nine parameters that are once or more often part of this top five are *c*, *Kext*, *KsatHorFrac*, *M*, *RootingDepth*, *Sl*, *Swood*, *thetaS* (θ_s), and *TT*. These parameters have a shared effect on both discharge and ET$_{act}$ simulations, although *RootingDepth* mostly affects the ET$_{act}$ simulations (Table 3), as it directly influences the maximum depth that can be used for water uptake in the evapotranspiration module.

c, *KsatHorFrac*, *M*, and θ_s are sensitive parameters as they influence either the available water storage or the fluxes between layers and cells. From that perspective, we expected *KsatVer* to be part of these sensitive parameters as well. *Kext*, *Sl*, and *Swood* are parameters that are used in the interception module by making use of the LAI maps. This affects ET$_{act}$, and through ET$_{act}$ the runoff ratio is altered affecting discharge. The sensitivity of this parameter is thus also related to the land cover. Since all three subbasins have a high fraction of forest, interception starts to play a bigger role leading to an expectedly higher sensitivity of these parameters.

Most of the sensitive parameters have an applied PTF to spatially estimate the parameter values. The two remaining sensitive parameters without a PTF are *KsatHorFrac* and *TT*. Both parameters have a higher degree of conceptualization than the more physically based parameters that do have a PTF. Because of this, it is challenging to find a point-scale PTF from literature with which the parameters can be estimated. Ideally, proper transfer functions are derived for these parameters. As this is outside the scope of this study, default parameter values are used for the model runs: 250.0 for *KSatHorFrac*, a value in between the range of values generally used for TOPKAPI and G2G (Todini & Ciarapica, 2002; Bell et al., 2007), and 1.3 °C for *TT* (Tobin et al., 2013). Hence, with respect to the first subquestion, most sensitive parameters of wflow_sbm are covered by a PTF but not all. In that case, a default value could be applied based on literature.

4.2. Validation of wflow_sbm Model for the Rhine

4.2.1. Discharge

For most gauging stations in the central and northern parts of the basin, KGE values range from 0.60 to 0.90 (Figure 3a). In this figure, an overview is given of the reached KGE (including *r*, α, and β) per river in the Rhine basin. Most of the Rhine tributaries have more than one discharge station. For each tributary, only the station with the largest standard deviation in discharge is displayed in order to have only one station per tributary in the figure, as these locations generally correspond to the river outlets.

Over the main course of the Rhine, KGE values fluctuate between 0.62 in Switzerland and 0.82 close to the Dutch-German border. The lower KGE values upstream in the main course of the Rhine are caused by a bias toward too low simulated discharge volumes in this region (Figure 3a), something we also see in the hydrograph for 2011–2015 of the Upper Rhine (KGE = 0.62 at Basel; Figure 4), a location which transports

Table 3
Results of the Parameter Sensitivity Analysis

| | Elsenz | | Obsi | | Omos 2 | | |
Parameter name	Q	ET	Q	ET	Q	ET	PTF
Soil parameters							
c	15	5	15	8	15	8	✓
KsatHorFrac	6	11	7	9	5	12	
KsatVer	6	12	9	11	9	14	✓
M	4	1	3	1	6	1	✓
SoilThickness	10	8	12	6	12	9	✓
thetaR	13	10	14	12	13	10	✓
thetaS	8	4	10	5	11	7	✓
Transpiration							
CapScale	17	17	17	17	17	17	
rootdistpar	16	16	16	16	16	16	
RootingDepth	14	2	13	3	14	2	✓
Interception							
Kext	5	9	5	10	4	6	✓
Sl	3	6	4	7	2	5	✓
Swood	1	3	2	2	1	3	✓
Flux partitioning							
InfiltCapPath	17	17	17	17	17	17	
InfiltCapSoil	17	17	17	17	17	17	
MaxLeakage	9	13	11	15	10	15	
PathFrac	17	17	17	17	17	17	✓
Routing							
N	17	17	17	17	17	17	✓
N_River	17	17	17	17	17	17	✓
Snow							
TT	2	7	1	4	3	4	
TTI	11	14	8	13	7	11	
WHC	12	15	6	14	8	13	

Note. Shown are the rankings from highest to lowest sensitivity on both modeled discharge (Q) and evapotranspiration (ET) per subbasin, following Van Griensven et al. (2006). The top five most sensitive parameters per subbasin and flux type are highlighted in blue. Parameters with the same sensitivity receive the same ranking.

all water of the Alpine basins. Especially during spring and summer, the discharge volume is sometimes highly underestimated with local differences of 500–1,000 m^3 s^{-1}. Going downstream, KGE values increase to 0.80 for the Lower Rhine at Emmerich (0.82 for the full period; see Figure 3). The volume difference of the Upper Rhine remains noticeable with slightly underestimated spring and summer discharges. However, due to the addition of water from non-Alpine headwaters, which do not have the aforementioned discharge volume bias, this effect is less pronounced in the results downstream.

This effect in the Alps already starts in the simulations for the headwaters in this area, with KGE values < 0.4 in the southwest of the area. For these headwaters, simulated discharge volumes are generally too low, as pronounced in the bias term (< 0.7). Also, discharge peaks are often underestimated. For instance, the Thur basin in the Alpine region (KGE = 0.51, Figure 4) has often highly underestimated peaks, and similar to the results in the Omos 2, the recession after a peak is slower than in the observations.

Most of the Alpine headwaters are supplying water to the reservoirs in the south of the Rhine basin, so the simulations of the lake levels should be influenced by the upstream simulations. This persists into the main
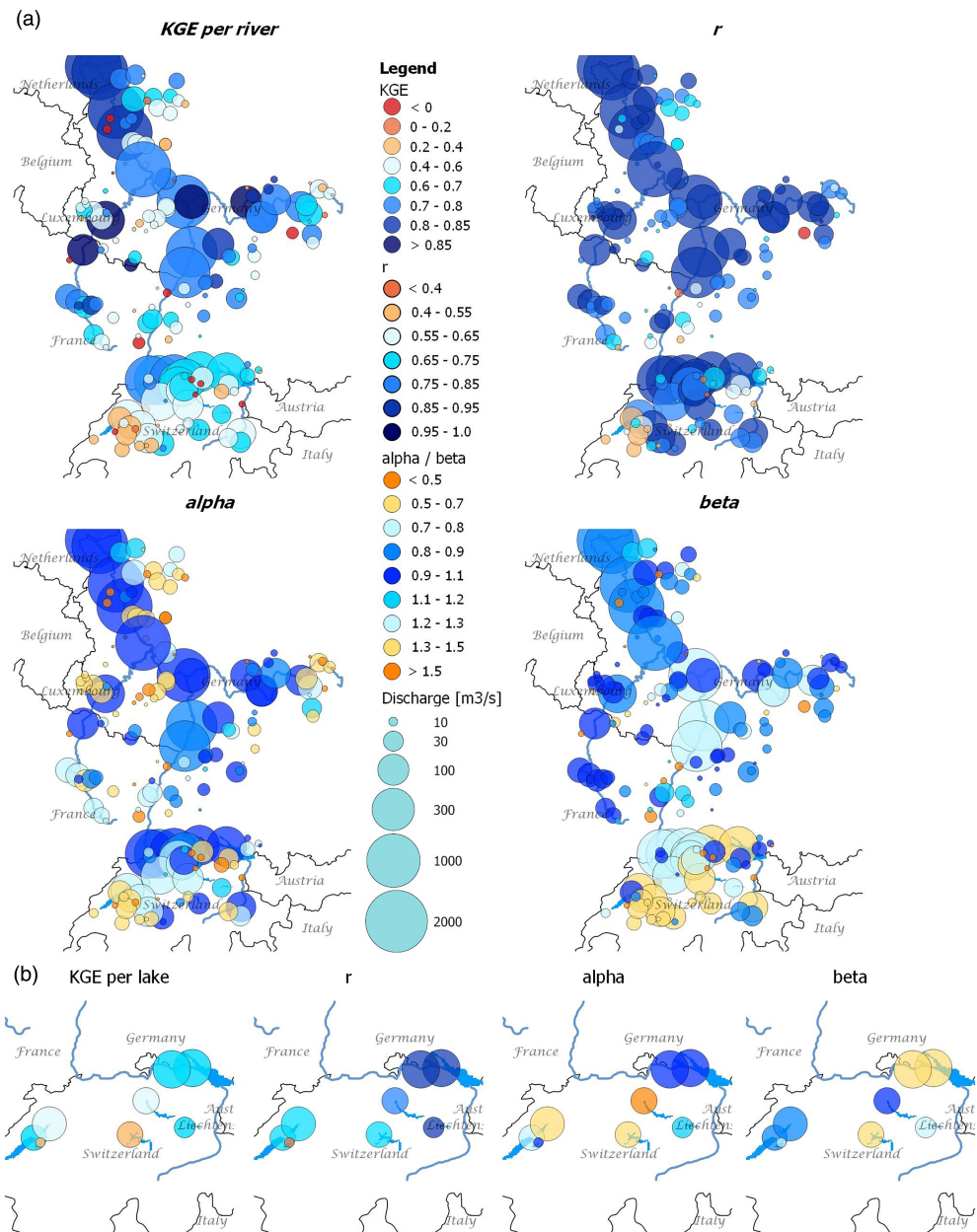
Figure 3. (a) Attained KGE per discharge station, split in the r, α, and β terms as described by Gupta et al. (2009). The size of the circles gives an indication of the mean discharge flux measured at that discharge station, while the colors display the reached values. Per tributary and if available, one location is displayed; this is the station with the highest standard deviation in observed discharge. KGE values and their decomposition are based on a comparison of the modeled discharge with discharge observations for the period 1999–2015. (b) Similar to (a) but for the simulated lake levels (bias term is based on subtracting the minimum lake level of the data set).

course of the Rhine, as the reservoirs are an important source of water to the Rhine in this region. For the lakes in the east, a bias is present indicating on the volume difference we also saw in the discharge simulations (Figure 3b). This volume difference is also present in the SWE estimations for snow and glaciers in the Alps (Figures S13–S15 in the supporting information). In the southwest, however, the bias in the lake level simulations is less. Here, not only a volume difference but also mismatches in the lake operation schemes (see Figure S3 in the supporting information) and in the timing and magnitude of the river discharges into these lakes (Figures S10 to S12) can cause the differences in simulated lake levels.

Model simulations for the river Moselle and its tributaries (west of the figure and mostly in France), and part of the Main plus its tributaries (east of the basin), give relatively high efficiencies with KGE values often
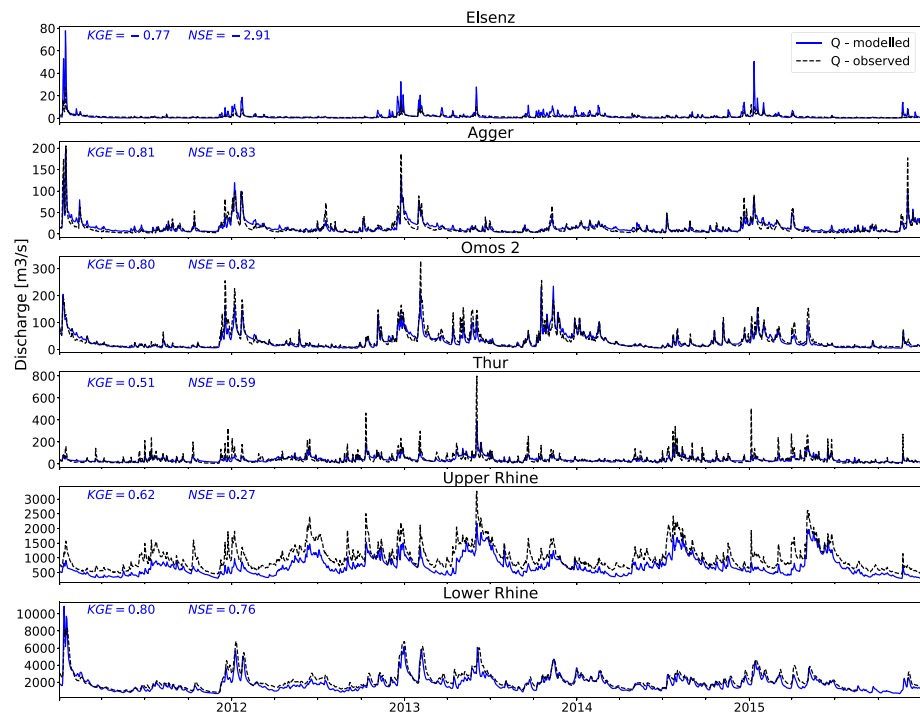
Figure 4. Hydrographs of discharge simulations with wflow_sbm for four subbasins of the Rhine (Elsenz, Agger, Omos 2, and the Alpine Thur) and two locations in the main course of the upper and lower Rhine (Basel and Emmerich). Hydrographs and metrics are shown for the period 2011–2016. Model simulations are indicated by blue lines and observations in black. Attained KGE and NSE values are displayed in the top left corner.

in the range 0.7–0.9. In the aforementioned regions, smaller tributaries sometimes have lower KGE-values (< 0.6). This is mostly pronounced in the α term of the KGE, with values often < 0.7, indicating on a difference in streamflow variability between observations and simulations. At these locations, the discharge simulations generally do not fully capture the quick discharge peaks after a rainfall event, while the baseflow is higher than observed. r and β on the other hand generally have values closer to 1.0 indicating on both a high correlation and a low bias between observed and simulated discharge. Especially in the Moselle, most model simulations are unbiased.

Focusing on a couple of the headwaters, discharge simulations for both the Agger (Sieg catchment) and Omos 2 (Moselle catchment) result in KGE values of, respectively, 0.81 and 0.80 (NSE is 0.83 and 0.82). Summer baseflow is often well captured for these basins, but most discharge peaks are somewhat underestimated for both catchments, generally followed by a too slow recession. For the Elsenz (Neckar catchment), the performance is less with a KGE of −0.77 (NSE = −2.91). The latter subbasin, Elsenz, does not have a station at the outlet, but it has a gauging station in the middle of the catchment at a tributary of the main watercourse, which makes the contributing area even smaller, while the catchment is already small with 539 km^2. The discharge simulations for this basin generally contain overestimated discharge volumes and peaks.

Hence, with the current model setup, we were able to reach average to good model performance in the middle and downstream region of the Rhine River basin. The Alpine region, in the south of the basin, is an exception to this due to a clear bias in the estimated discharge amounts and to a lesser extent due to not well captured discharge variability of the peaks and recession rates.

4.2.2. Actual Evapotranspiration

For the entire Rhine basin, the spatial patterns of ET$_{act}$ simulations directly reveal that modeled ET$_{act}$ by wflow_sbm is systematically higher (542 mm yr^{-1}) than the DMET modeled ET$_{act}$ (427 mm yr^{-1}), with a relative "bias" of 1.27 (Figure 5). Spatial patterns show a degree of correspondence in the higher Alps in the south and close to the catchment outlet. A band of higher ET$_{act}$ in the flatter valley in northern Switzerland is also present in both simulations, although the simulation of wflow_sbm is higher for a larger region than just a narrow band in the north of Switzerland, as is the case for DMET.
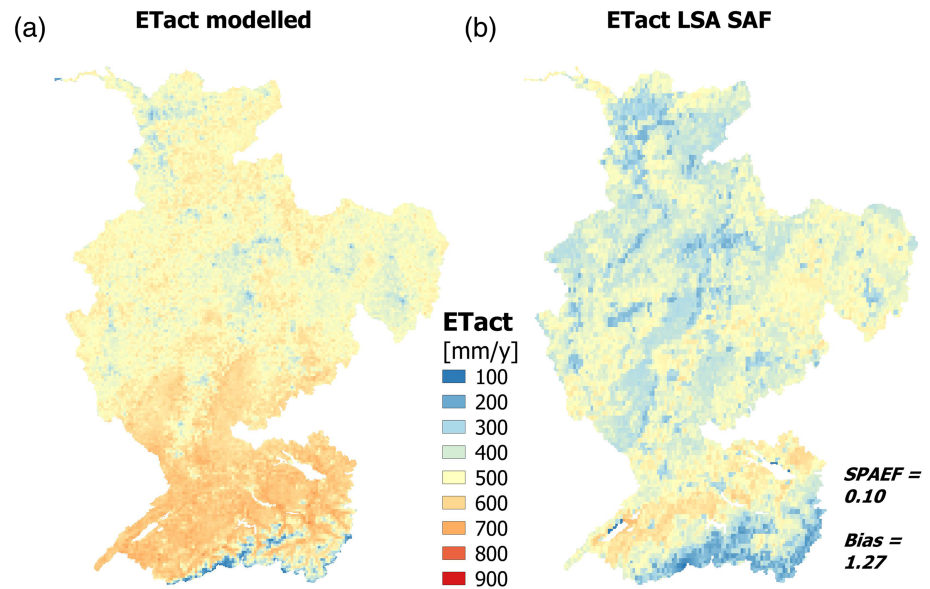
Figure 5. A comparison between (a) modeled yearly averaged ET$_{act}$ simulations (upscaled to a resolution of 3 km) and (b) DMET ET$_{act}$ simulations (Trigo et al., 2011).

Between other regions, there are more differences, leading to a SPAEF of 0.10. Although the overall spatial variability is quite similar ($\chi = 0.72$), the correlation and clusters of spatial patterns differ ($\phi = 0.27$ and the histogram intersection, $\psi = 0.55$). Especially, the Rhine valley (see also Figure 1) shows a clear difference between the two models. For DMET, yearly ET$_{act}$ simulations are higher in the Rhine valley than on the two forested ridges next to it. For the wflow_sbm simulations, this is exactly the opposite.

In Figure 6, a time series of subbasin spatially averaged daily ET$_{act}$ simulations are compared to DMET. For all basins, winter ET$_{act}$ derived with wflow_sbm is higher than DMET. For the remaining seasons, the differences between the two models are smaller. Omos 2 (KGE = 0.62) is an exception to this, with almost continuously higher ET$_{act}$ by wflow_sbm (bias = 1.32). Other than that, day-to-day catchment-averaged patterns are more in agreement than it was the case for the spatial comparison in Figure 5, with KGE values around 0.7 ($\rho \approx 0.8$).

A clear discrepancy is present between modeled ET$_{act}$ and DMET simulates for all three basins from July to August 2013. During a drier period in these months, ET$_{act}$ simulated by wflow_sbm shows reduced ET$_{act}$ for most of the period. The simulated ET$_{act}$ from DMET does not show this behavior. Either the wflow_sbm model overestimates the reduction in evaporation as a result of limited soil moisture or the DMET model did not apply a suitable reduction. If the difference stems from the former, (in this case) likely either the water storage was too low, for example, due to the limited soil depth of 2 m, or the rooting depth was too shallow. In section 5.2.2, we elaborate on the different processes between wflow_sbm and DMET used for estimating the soil moisture content.

4.3. Scalability of the Model
4.3.1. Parameter Estimates on Four Resolutions
Figure 7 illustrates obtained parameter maps for the saturated conductivity (*KsatVer*) and the saturated water content (θ_s), in combination with probability density distributions of the obtained parameter values. Both the resulting parameter maps of the saturated conductivity (a–h) and the saturated water content (i–p) indicate on a preservation of the spatial parameter fields on the four resolutions. This is also illustrated by the mean values and standard deviations of the probability density distributions, which are unchanged when moving to coarser resolutions: $\mu = 6.31$ and $\sigma = 1.01$ (log mm day^{-1}) for the saturated conductivity and $\mu = 0.46$ and $\sigma = 0.03$ for the saturated water content). However, for *KsatVer*, a small decrease of μ (from 6.31 to 6.30 log mm day^{-1}) and of σ (from 1.01 to 1.00 log mm day^{-1}) is present.
4.3.2. Consistency of Fluxes and States on Four Resolutions
ET$_{act}$ fluxes are well preserved on all four resolutions (Figures 8a–8j), with relative errors between the highest resolution and the coarser resolution that are generally < 10% (Figures 8e–8g). Occasionally, relative errors
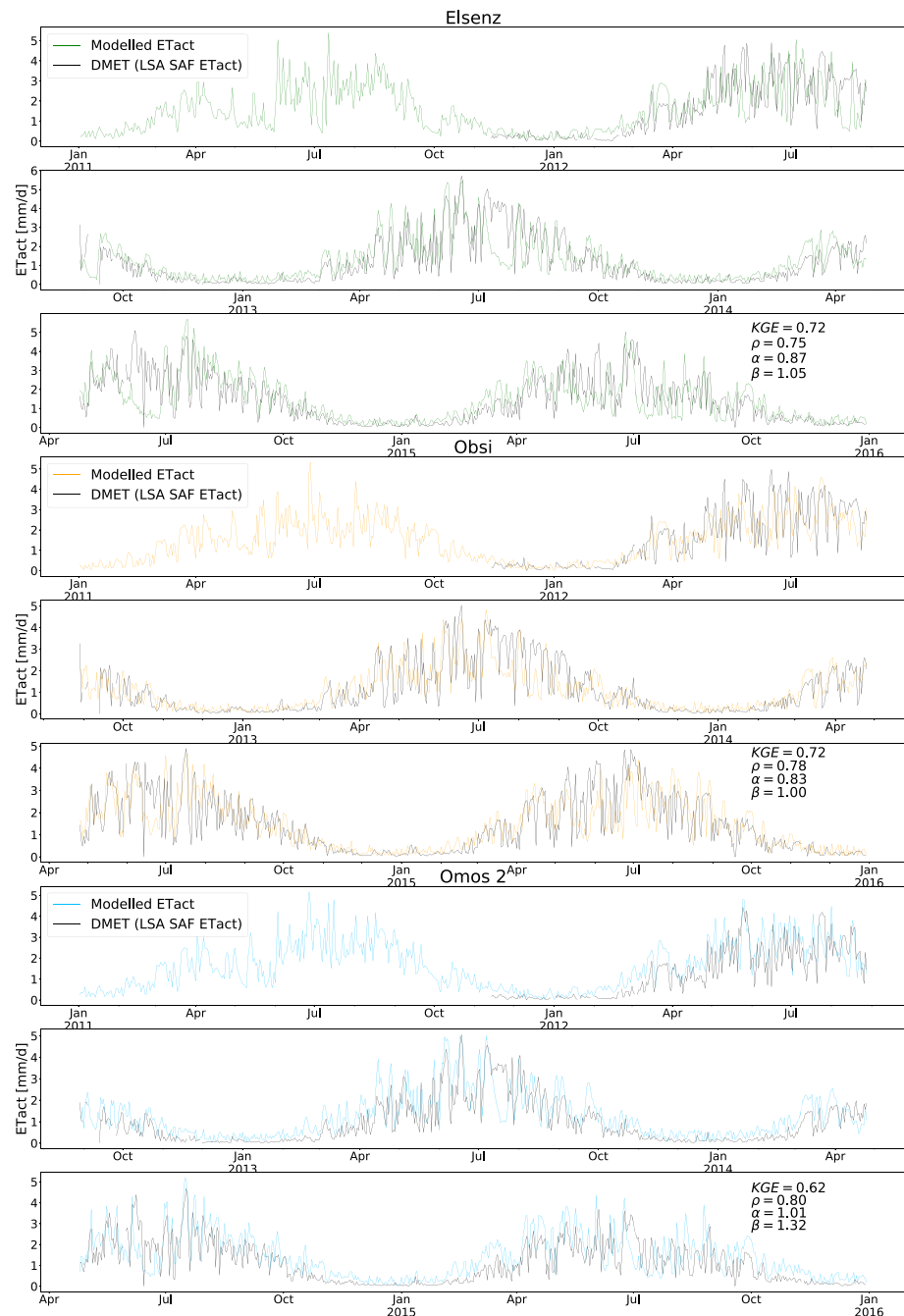
Figure 6. Catchment-averaged daily ET_{act} simulated with wflow_sbm for three subbasins of the Rhine for the period 2011–2016. These aggregated daily ET_{act} simulations are compared to DMET ET_{act} (black line). Green lines indicate the modeled ET_{act} for the Elsenz, in orange for Obsi, and in blue for Omos 2.

of $\pm30\%$ are present. This mostly occurs in regions with an average daily modeled ET_{act} flux around 0.5 mm day^{-1}, for example, the higher Alps and the northern Rhine valley. For the Alps, these differences can be caused by glaciers and snow processes that are not well scaled, due to the absence of PTFs for the parameters of these modules. As most variability seems to take place locally (from pixel to pixel) and not necessarily per region, Figures 8h–8 j illustrate the relative errors of the catchment-averaged ET_{act} simulations. The relative errors in these figures are for all subbasins close to zero, indicating that ET_{act} fluxes remain preserved on all four resolutions.
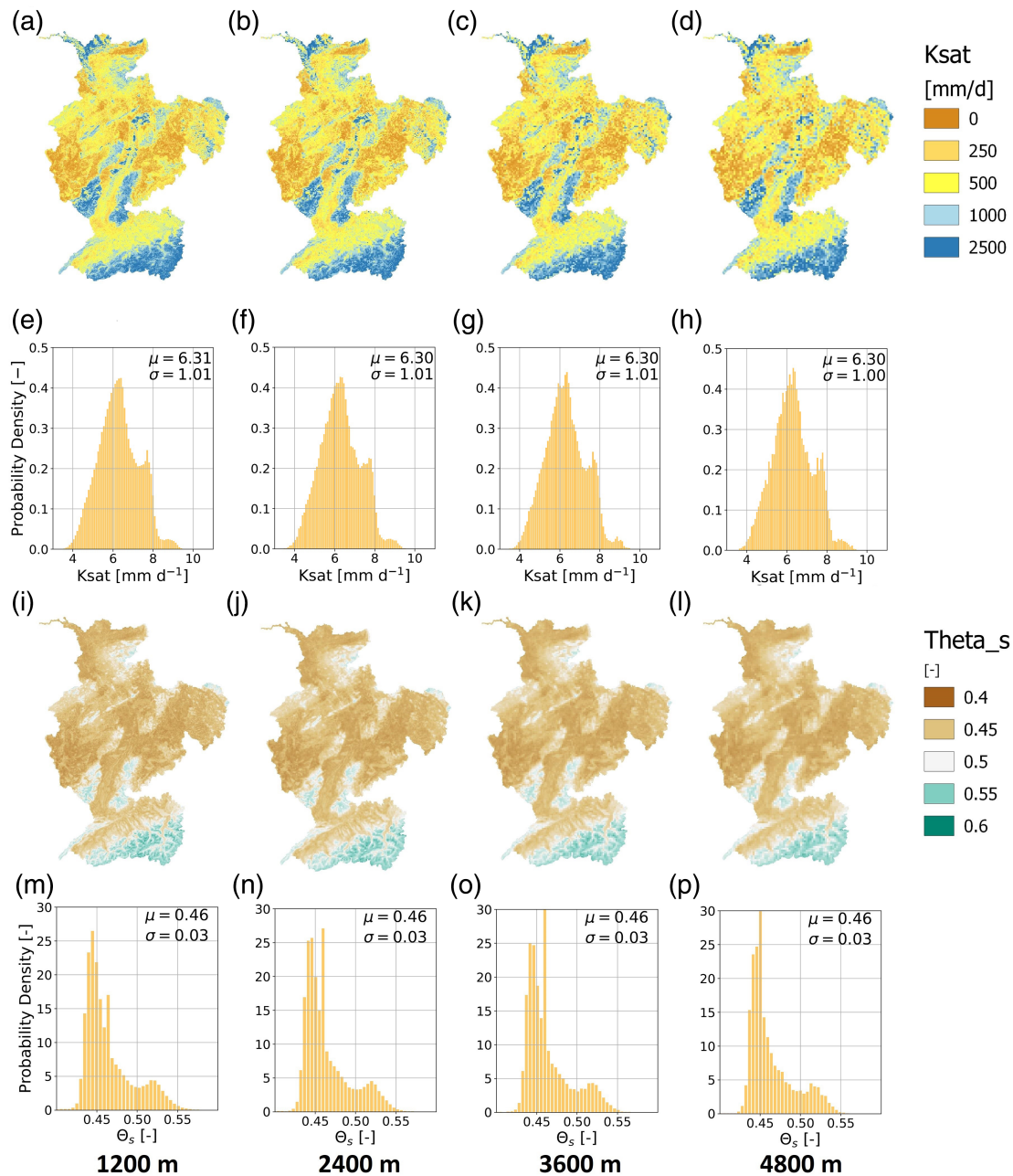
Figure 7. Parameter estimates at four resolutions for *KsatVer* and θ_s. (a–d) Parameter estimates of *KsatVer* with increasing resolution from 1.2 to 4.8 km. (e–h) Histograms of the natural logarithm of the KsatVer parameter values; histograms match with the parameter maps on top of them. (i–l) Parameter estimates of θ_s at the same four resolution. (m–p) Similar to the previous histograms but for θ_s.

Flux preservation is certainly not everywhere the case for the recharge fluxes (the net flux of downward transfer and capillary rise; see Figure 2) in Figures 8k–8n. Especially in regions with recharge fluxes just above or below 0.0 mm day^{-1}, the relative errors (o–q) often exceed the ±50%. However, absolute errors are generally low (0.0–0.1 mm day^{-1}) in those regions and mostly take place close to river cells. This is likely caused by the scaling of river cells, which is well visible between the maps of Figures 8k (1,200 m) and 8n (4,800 m). The incorrect scaling causes a slight shift in the location of river cells and the subsurface flow network, inevitably leading to wetter or drier cells around the river cells than on another modeling resolution. Around these river cells, the relative error is highest (Figure 8q), while in other regions the relative error is minimal. The resulting speckled pattern, however, reduces when the catchment-averaged fluxes are compared in (r–t). There, relative errors are more often < 10% and around 30% in the subbasins around the main
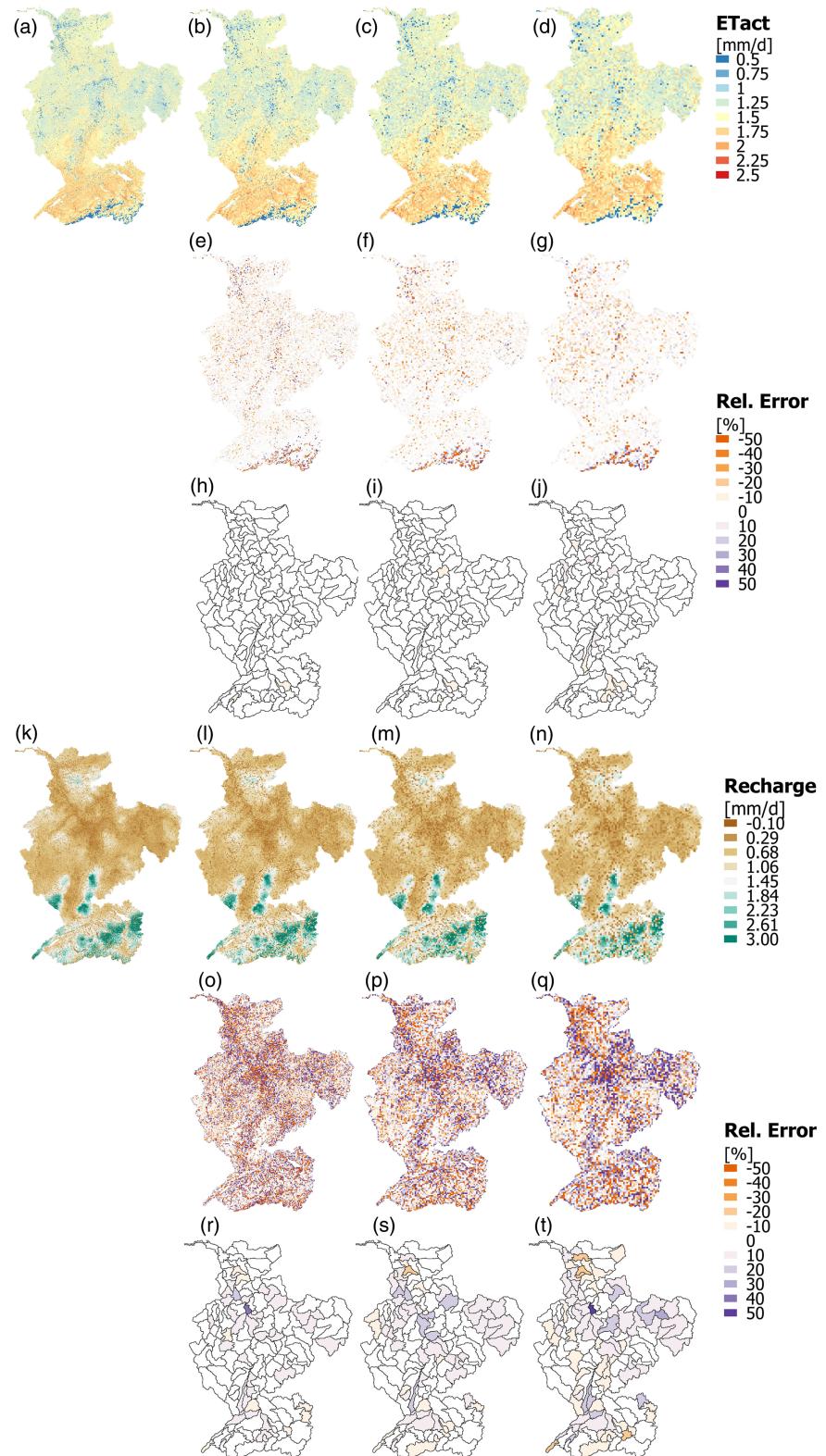
Figure 8. Simulations of daily averaged ET$_{act}$ on four resolutions, (a) 1.2, (b) 2.4, (c) 3.6, and (d) 4.8 km. (e–g) The relative error per grid cell between one of the coarser resolutions (b–d) and the simulations on 1.2 km (a) after upscaling these simulations to one of the coarser resolutions. (h–j) Same as (e)–(g) but catchment-averaged fluxes are used instead of fluxes per grid cell. (k)–(n) The daily averaged recharge fluxes on the four resolutions. (o)–(t) Same as (e)–(j) but then for the recharge fluxes.
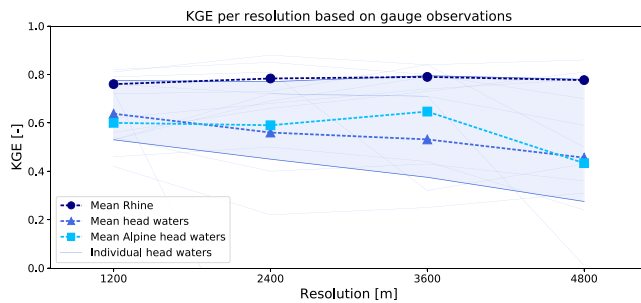
Figure 9. KGE per resolution as derived with model simulations and observations from 19 gauges. Shown are the mean KGE for 3 gauges in the main course of the Rhine (dark blue), 3 gauges in Alpine head waters (light blue), and 13 gauges in headwaters in the middle and downstream areas of the Rhine basin (blue). The shaded blue area is the area in between the 25th and 75th percentiles (the interquartile range - IQR) for the middle and downstream headwaters.

course of the Rhine, where the recharge fluxes are closer to 0.0 mm day^{-1}. This mainly applies to the central Rhine valley, the river Main, and the course of the Rhine after the tributaries of the Main and Moselle have joined it. These are regions where the drainage density is relatively high.

In Figure 9, performances of modeled discharge, indicated with KGE, are given at the four model (Level 1) resolutions as an average performance for the main course of the Rhine (dark blue), for 13 headwaters in the middle and downstream parts of the basin (blue) and for 3 Alpine headwaters (light blue). Discharge simulations in the main course of the Rhine remain constant with an average KGE over three gauges of 0.78 on all resolutions. This is, however, not the case for simulations in the (Alpine) headwaters. The averaged attained KGE for the 13 subbasin decreases from on average 0.64 to 0.46 between the finest (1.2 km) and the coarsest (4.8 km) resolution. For the three Alpine headwaters, this decrease is almost absent until a resolution of 3.6 km, followed by a quick decrease toward a resolution of 4.8 km. Hence, although simulated discharge scales well for the larger rivers, discharge simulations are not fully consistent for the headwaters with wflow_sbm and the approach in this study.

5. Discussion

The transition from lumped to gridded models enables us to take advantage of spatial data and is important for a variety of modeling applications, in particular, to study climate and land use changes (Fatichi et al., 2016). As stated in section 1, moving to distributed modeling concepts has consequences and comes at a price regarding parameter estimations (Archfield et al., 2015; Beven, 2006; Bierkens, 2015; Clark et al., 2016; Mizukami et al., 2017; Paniconi & Putti, 2015; Samaniego et al., 2010). In this study, we were able to parameterize most sensitive components of the wflow_sbm model using literature PTFs derived from laboratory experiments with point-scale samples in a bottom-up approach. Still, in the current scientific debate, there is no consensus on the matter of using either a bottom-up or top-down approach in setting up hydrologic models. Arguments against a bottom-up approach are that this results in overly complex models and that processes on the data-driven conceptualization scale, for example, the PTFs derived on the point scale, may not be representative on the actual modeling scale (Beven, 1989; Blöschl & Sivapalan, 1995; Sivapalan et al., 2003). With the increased availability of (remotely sensed) spatial data, meteorological forcing with both high spatial and temporal resolution, new upscaling procedures (e.g., Samaniego et al., 2010), and high-resolution models, it can be argued that this makes a bottom-up approach more feasible.

However, the use of so-called point-scale PTFs, as used in this study, is still debatable. Samaniego et al. (2017) even state that these PTFs should not be used at all beyond their derivation scale (often 100 cm^3). They support this statement based on an analysis with PCR-GLOBWB (Bierkens & Van Beek, 2009; Van Beek et al., 2011) and Noah-MP (Niu et al., 2011), which are parameterized with ad hoc implementations of PTFs. An important difference with this study is that the model parameters were originally not well upscaled (Noah-MP) or even derived at the model resolution (PCR-GLOBWB) when the point-scale PTFs were applied. In this study, we have focused on deriving the parameters on the original data resolution (Level 0) followed by upscaling with suitable upscaling operators to the model resolution (Level 1). In essence, when this two-step approach (Samaniego et al., 2010) takes place in the appropriate way, the process of upscaling the parameter estimates should be independent of the chosen parametrization (i.e., calibration and use of PTFs) on the Level 0 scale. Note, however, that actual model performance can still be improved by making use of a calibration procedure.

The question that then remains is whether point-scale PTFs can be used to obtain parameters at the current Level 0 scale (e.g., 250 m for SoilGrids Hengl et al., 2017), also with regard to the uncertainty of the chosen PTFs. We expect this to be parameter specific; for example, the saturated conductivity varies more on small scales than the soil depth. A focus on the parametrization (Level 0) scale and sensitivity to the chosen PTF is therefore recommended in future studies with point-scale PTFs. Point-scale PTFs have the advantage that they require no further model calibration and therewith leaving out any model and forcing-related dependency of the results. In fact, these transfer functions are derived from laboratory experiments with

soil samples and are therefore still closely linked to soil properties. To have a better understanding of the strengths and limitations of using point-scale PTFs, we think it is of interest to compare a model parametrization with calibrated transfer functions, following, for example, Samaniego et al. (2010) and one with the implementation of point-scale PTFs as done in this study.

We think that with the increasing spatial resolution of soil and vegetation data sets, in combination with high (spatial and temporal) resolution models that move toward better physical representations of hydrologic processes, the use of these point-scale PTFs becomes more feasible. Certainly, with the results obtained in this study, we see a clear reason to keep exploring the potential of such an approach.

An advantage of this approach is that it shifts the focus toward the model processes and its limitations. This is something that, in our opinion, is not present yet in other papers that included the MPR approach. This focus makes it possible to specify improvements for model parameters and model structure for both increased model performance and a better scalable model. In the following sections of the discussion, we focus on these improvements by reflecting on the subquestions that were posed in section 1.

5.1. Parameter Sensitivity, Estimates, and Upscaling Rules

In this section, we focus on the PTFs used in wflow_sbm that cover the sensitive parameters of this model and the parameters that are not covered by a transfer function 5.1.1. Possible improvements in the parameter estimates are discussed in section 5.1.2.

5.1.1. Parameter Sensitivity Analysis

In the sensitivity analysis, we have found nine sensitive parameters that should have a parameter estimation, either via PTFs or via calibrated transfer functions. Two of them did not have an applied (pedo)tranfer function. Although this is outside the scope of the current study, a transfer function for these parameters is needed in the absence of a point-scale PTF. The search for and calibration of transfer functions for the snow module parameters is then an option. That this is possible for these parameters has already been shown by Samaniego et al. (2010) and Kumar, Samaniego, et al. (2013).

The other sensitive parameter without a PTF is *KsatHorFrac*. This multiplication factor applied to the vertical saturated conductivity, which is generally larger than 1, has a pronounced effect on the lateral subsurface flows and via that way on modeled discharges (see also section 5.2.1). Although multiple PTFs are available for the vertical saturated conductivity in literature (e.g., Van Looy et al., 2017), there are no PTFs available in literature for this multiplication factor that may compensate for anisotropy resulting from the point-scale PTF to estimate *KsatVer*. The estimation of the horizontal saturated conductivity is therefore likely not representative for larger-scale horizontal saturated hydraulic conductivities at the model resolution (with in reality smaller hill slope flow length scales). To allow for no further calibration, we have chosen to fix this parameter to a default value. Nevertheless, for future model improvement, a transfer function or calibration of this parameter is recommended.

Kext, *Sl*, and *Swood* parameters that are part of the interception module were found to be among the most sensitive parameters of the model. In section 4.1, we gave a reason for this sensitivity, as it highly impacts evapotranspiration and with that discharge. In addition, the temporal scalability of these parameters (here run on a 6 hr time step) is possibly an issue too. The wflow_sbm model switches from the analytical Gash model (Gash, 1979) on daily time steps to a modified Rutter (Rutter et al., 1971, 1975) model on subdaily time steps. This can already cause nonscalable behavior, especially for interception related parameters (Ficchì et al., 2019), possibly leading to a higher sensitivity to these parameters on a 6 hr time step, as this is also at the transition between the two approaches. An improved interception module that uses a constant approach on different time scales is therefore recommended.

5.1.2. Parameter Estimates

Using point-scale PTFs from literature, a large part of the measured variability (expressed in relatively high KGE/NSE values) is explained. This minimizes the need for further calibration, although of course an MPR calibration could potentially further improve the outcomes. This is left for future work. The advantage of the approach taken here is that the transfer functions are no longer constrained to the model and regional discharge data, giving, in theory, even more potential for regionalization. However, also PTFs have a constraint, which are the field samples they are based on. These field samples are generally limited to certain regions in the world, which makes the empirical relationships derived in the laboratory not necessarily representative for all river basins. For the estimation of especially θ_s, θ_r, *KsatVer*, and *c*, many more PTFs are available. So the choice of a modeler for a certain point-scale PTF can then depends on the area of interest.

In addition, some of the point-scale PTF implementations can still be improved. By making use of *KsatVer* estimations at seven depths and a simple exponential fitting, a rough estimation of the *M* parameter is made. Conceptually, *M* is the exponential decay of *KsatVer* with depth, so this approach suits the concept. However, with the wealth of soil information on seven depths and therewith also *KsatVer* estimations on seven depths, the *M* parameter is not strictly necessary. For shallow soils, the saturated conductivity with depth can also be estimated with the available information and in that way also allow for, for example, increasing saturated conductivity values with depth, instead of only a decay.

Moreover, N_{river}, Manning's roughness coefficient for water flow in watercourses has not been found to be a sensitive parameter, but it may become more important for larger river systems such as the main course of the Rhine. In this study, we have used a method which relates the Strahler order of a river cell to a coefficient value for N_{river} (Table 1) based on Liu et al. (2005). This method is, however, not often tested, and therefore, it is uncertain whether these values are universally applicable or only locally applicable.

5.2. Validation of Wflow_sbm Model for the Rhine

In this section, we discuss the resulting quality of the wflow_sbm model on the highest resolution of interest (1,200 m) as assessed on simulated discharge 5.2.1 and evapotranspiration 5.2.2 after the parameter estimations and upscaling procedures were applied.

5.2.1. Discharge

The results at Lobith, at the Dutch-German border, are comparable to results found with the (MPR calibrated) mHM model in an earlier study for the Rhine by Rakovec et al. (2016), although note that the used forcing was different in this study (supporting information Figure S8). With a KGE just under 0.9 for both models, discharge is generally well simulated. One difference is that the first peaks during fall seem to be better captured by wflow_sbm, as the results with mHM give too flashy responses with a high recession rate afterward. Winter peaks are reasonably well captured by both models in the comparison.

The results are also comparable to discharge simulations by Van Osnabrugge et al. (2017) with wflow_hbv (a distributed version of HBV within the wflow framework), where five model parameters were derived with a basin by basin GLUE analysis approach. In that study, the same meteorological forcing was used. In the Alpine headwaters, lower KGE values were attained as well. Discharge performance in the river Main is better than for wflow_hbv, while the opposite is true for the river Ahr (central region of the basin) and the river Ruhr (northeast). Other regions are similar in terms of attained KGE for discharge simulations; see also Van Osnabrugge et al. (2017).

Although discharge simulations and therewith model performance are promising with this modeling approach, discharge simulations are insufficient in the Alpine region. We see five likely reasons for this behavior of the model: (1) incorrect lake "operation" representation, (2) used uncertain model parameters, mainly *KsatHorFrac* and snow parameters, (3) the model forcing in this area, (4) the chosen model resolution, and (5) the river and drainage network derivation procedure.

In Figure 3b, we saw that some of the lakes in Switzerland are not well modeled, resulting in lower KGE values. Additional time series of lake levels are present in the supporting information (Figure S3). Part of this can be attributed to a mismatch in simulated discharge volumes and timing from the upstream headwaters, but, for example, the Murtensee is an example of a reservoir for which the release of water clearly occurs in the wrong season leading to a clear mismatch between the observed and modeled lake levels. Improving the reservoir operation schemes, which were obtained from the operational Rhine model, is therefore a necessary additional improvement.

It is obvious that the used approach of a uniformly applying default snow parameter values is insufficient, as also the SWE estimations are on average 25–50 % lower than the SLF estimates (see also Figures S13–S15). Ideally, these parameters are estimated with transfer functions. Day-degree parameters are hard to relate to physical characteristics (Seibert, 1999), although some studies have tried to link the day-degree factor to land cover, elevation, slope, and aspect (e.g., Dunn & Colohan, 1999; Kuusisto, 1984; Semádeni-Davies, 1997). As a calibrated transfer function, relating the day-degree factor to land cover was already done by Kumar, Samaniego, et al. (2013).

In addition, *KsatHorFrac* was found to be a sensitive parameter. This parameter has a pronounced effect on the partitioning of discharge in quick runoff and baseflow. A higher value for *KsatHorFrac* leads to a higher baseflow, lower peaks, and a somewhat slower recession after a discharge peak. Besides the need for a

calibrated transfer function for this parameter, the uniformly applied value of 250 may have been too high for many regions in the Rhine basin (see, e.g., Figure 4). Especially for the Alps, quick responding catchments are often not well modeled with too high baseflows and too low or even missed discharge peaks. In this region, a lower value for this parameter can increase model performance. This is tested for the Thur basin (supporting information Figure S9), where four different *KsatHorFrac* values (10, 100, 250 and 1,000) are implemented. With decreasing *KsatHorFrac*, peaks get higher with steeper recession curves and generally a lower baseflow. For a *KsatHorFrac* of 10, the peaks that were highly underestimated in Figure 4 are even overestimated. With a calibration procedure, we expect that a value in between 10 and 100 will be found, leading to increased model performance for this (and similar Swiss) basin(s).

Mainly in the southwest of the Alps, forcing errors played a role. In this region, mostly located in Switzerland, the observation network used for the forcing is not dense enough to capture the high rainfall variability in this mountainous region. The result is an underestimation of precipitation, especially during winter, for this region compared to other precipitation data sets (Van Osnabrugge et al., 2017). Hence, besides the parameterization, this is a second reason for the mismatch between modeled and observed discharge in this region, especially concerning the volume bias during the winter period (October - March).

Within this approach, a high-resolution model on $1,200 \times 1,200$ m was used which led to discharge simulations that well resembled the observations in most of the Rhine basin. However, for the Alpine region, this grid cell resolution may still be too large to well capture processes such as the lateral subsurface flow representation. It is possible that other parameters, for example, *KsatHorFrac*, are compensating for this now.

Another issue related to resolution is the derivation of the river and drainage direction and network. This derivation was conducted on the model resolution, while ideally, this takes place on the DEM resolution, followed by an upscaling procedure keeping the subgrid information available on the model resolution. What we see with the current model is that discharge and subsurface lateral flow simulations are not scale independent (Figures 9 and S7). This is certainly related to the fact that the river network is not properly scaled. Section 5.3 focuses further on this scalability. For the Rhine and especially the Alps, it is needed to improve the derivation of river and drainage direction networks, for example, following Thober et al. (2019). This is currently under development.

5.2.2. Actual Evapotranspiration

In this study, we have compared modeled ET_{act} values with LSA SAF DMET estimates by Trigo et al. (2011). Note that this is a comparison of two models, and care should be taken when interpreting the results or drawing hard conclusions on the basis of this comparison. In our opinion, however, this is a valuable addition to the validation procedure of hydrologic models since both models estimate ET_{act} in a different manner. An important difference is that DMET estimates the plant available water with remotely sensed soil moisture status estimations, while in wflow_sbm, plant available water is the remaining precipitation from the forcing in the unsaturated buckets that are reachable by the plants roots. Hence, the driving boundary conditions for root zone water availability, that is, remotely sensed soil moisture or precipitation estimates, can already be substantially different, leading to, for example, the bias between the two model estimates.

Simulated average yearly ET_{act} differed considerably between the models with 427 mm a year for DMET and 542 mm a year with wflow_sbm. Hurkmans et al. (2008, 2009) have found a yearly average of 659 mm from lysimeters for the Rheindahlen (near the Dutch border), 541 for the Rietholzbach (part of the Thur basin), and on average for the land use types deciduous forest, grassland, and crops values of 491, 659, and 398 mm. This indicates that DMET estimates are too low for the area. Nevertheless, day-to-day variability of ET_{act} for the three subbasins is comparable for both models (Figure 6).

5.3. Scalability of the Model

In this section, we focus on the scale (in)dependency of the resulting wflow_sbm model. How important were the upscaling rules 5.3.1 and what is still necessary to reach flux preservation for especially the discharge related fluxes 5.3.2.

5.3.1. Upscaling Rules

The application of appropriate parameter-specific upscaling rules is of key importance within this approach. A good upscaling rule is found when the upscaling of the parameters leads to consistent parameter fields across scales, as indicated with the constant mean and standard deviation of the parameters in Figure 7 (see also Figure 3 in Samaniego et al., 2017). Both in Figure 7 and in the supporting information Figures S4–S6,

some examples are given of the effects of the upscaling rules on obtained parameter fields. The results show a high degree of consistency in the parameter fields. Therefore, we argue that consistent parameter fields on different resolutions are reachable with a combination of a priori PTFs and appropriate upscaling rules.

The results of this study have shown that saturated hydraulic conductivity (and lambda) fields are well upscaled with an arithmetic mean of their natural logarithm. This choice has followed from their log-normal distribution and the used PTFs which are formulated as an exponential function (Table B1). In practice, however, the difference between upscaling with the arithmetic mean of the natural logarithm and just the arithmetic mean of the normal values is small (but present; Figure S6). Possibly, this is caused by the high standard deviation in the parameter estimations, partly caused by the high natural spatial variability in the saturated conductivity, which makes the effect of different upscaling operators less pronounced.

In addition, saturated and residual water content parameters are upscaled with a harmonic mean in the mHM model (Kumar, Samaniego, et al., 2013; Kumar, Livneh, et al., 2013; Samaniego et al., 2010, 2017; Rakovec, Kumar, Attinger, et al., 2016; Rakovec, Kumar, Mai, et al., 2016). Within our approach, upscaling of these parameters has taken place with an arithmetic mean. In the supporting information (Figure S4), we have compared both approaches and they give similar consistencies in parameter fields on different resolutions, although with a slightly different mean for the two approaches. Hence, it seems that the chosen upscaling procedure (i.e., harmonic or arithmetic) of this parameter does not influence the consistency in the obtained parameter fields on different spatial scales. However, the choice for the upscaling procedure then depends on the nature and sub-grid variability of the parameter.

5.3.2. Flux Preservation on Different Resolutions

In theory, the choice of the right upscaling procedure per parameter should lead to the preservation of modeled fluxes and states on different spatial resolutions (Kumar, Samaniego, et al., 2013; Kumar, Livneh, et al., 2013; Samaniego et al., 2010, 2017). In this study, similar results are found for ET_{act} flux estimates on the four applied spatial resolutions (e.g., 0–10% in Figure 7 of Samaniego et al., 2017). Only on a subbasin scale, we have found similar results for recharge fluxes, while on the grid cell scale, the variability is higher.

In contrast to those results, we have not found flux preservation for discharge related fluxes (e.g., river runoff and subsurface lateral flows), especially for headwaters (Figures 8 and S7). This is particularly the case for small basins (mostly headwaters) that rely on well scaled slopes and well scaled river and drainage networks. In areas where the network is dense and not well scaled to the model resolution, this leads to a river network and lateral subsurface flows that have a slightly different direction or location (in case of the network) than at higher resolutions, which can lead to large relative errors in spatially accumulating fluxes. This is well visible in Figure S7 of the supporting information.

For mHM, however, discharge simulations have given quite consistent results on both finer and coarser spatial resolutions, with a maximum efficiency at a simulation and calibration scale of 8 km (Kumar, Samaniego, et al., 2013; Samaniego et al., 2010). In addition, Thober et al. (2019) have recently updated the routing component of mHM to scale river routing correctly. Hence, this shows that it is possible to obtain discharge flux preservation on different spatial scales. However, that this is possible with a model that allows for lateral subsurface flows has not been shown yet. For wflow_sbm, it requires a structural change in the (current) automated process of slope, river, and drainage network derivation from, for example, DEM information. This could be a procedure similar to Thober et al. (2019). Ideally, this takes place on a subgrid scale, as the local drainage directions, determined at the model resolution, probably do no longer capture all drainage processes well on the coarser model resolution, leading to erroneous representations of rivers and drainage networks.

Finally, we have not tested the approach on finer resolutions than $1,200 \times 1,200$ m. Kumar, Samaniego, et al. (2013) have shown that fluxes remain more or less preserved when moving toward higher resolutions than the used calibration scale. Although this is not tested here, we expect to obtain similar results or even increasing model performance when it comes to simulation of discharge or lateral subsurface flows with the current version of wflow_sbm. This is based on the aforementioned representation of the river and drainage network, which is expected to be better on higher resolutions.

6. Conclusions

Moving toward high-resolution spatially distributed hydrologic models asks for a different approach in estimating parameter values. In this paper, we combined parameter estimates from point-scale PTFs with a

high spatial and temporal resolution model (wflow_sbm) for the Rhine basin. Following previous studies by among others Samaniego et al. (2010), Kumar, Samaniego, et al. (2013), Kumar, Livneh, et al. (2013), Rakovec, Kumar, Attinger, et al. (2016), Mizukami et al. (2017) and Samaniego et al. (2017), we set up the parameter estimates on the original data resolutions and upscaled derived parameter fields to various model resolutions by making use of suitable upscaling operators.

The objective of this study was to investigate the applicability of point-scale PTFs in combination with suitable upscaling operators for deriving seamless hydrologic model parameters and the preservation of fluxes across scales for a multiscale hydrologic model for the Rhine River. We focused on three aspects: (1) Can we cover the sensitive parameters of the wflow_sbm model with point-scale PTFs from literature? (2) To what model performance does this setup lead on the highest resolution of interest (1,200 m)? (3) How scale (in)dependent is the resulting model on four resolutions (1.2, 2.4, 3.6, and 4.8 km)?

With point-scale PTFs from literature, we were able to estimate almost all sensitive parameters of the wflow_sbm model. The two remaining parameters, together with the relatively insensitive parameters, were set to default values and were applied homogeneously over the entire Rhine basin. This gave us a model setup with parameter values, either estimated or fixed, which made it possible to model the hydrology of the Rhine basin without any further calibration, while obtaining similar performance as calibrated models (i.e., mHM and wflow_hbv).

The used parametrization of the model led to promising results. For most discharge gauging stations in the central and northern parts of the Rhine basin, KGE values ranged from 0.6 to 0.9. An exception to this result was the Alpine region, where lower KGE values were attained, especially in the southwest of the basin. For the greatest part, this could be attributed to a volume bias in the simulated discharge. This volume bias in the upper part of the basin transferred downstream in the main course of the Rhine, and we attribute this to a biased forcing in this region.

The validation of evapotranspiration simulates took place with a comparison with LSA SAF DMET estimates. Model simulates were systematically higher than for DMET with 115 mm yr^{-1}, although DMET was found to have too low estimates for the Rhine region compared to values from literature. Spatial patterns between the two models were somewhat similar for the Alps, northern Switzerland, and the downstream area of the basin. Between the other regions, however, many differences were present, especially in the Rhine valley and the surrounding hills (SPAEF = 0.10). Here, spatial patterns of higher and lower evapotranspiration were often the opposite of the DMET estimates. Contrarily, catchment-averaged temporal dynamics for three subbasins were better with KGE values around 0.7. Hence, although the temporal dynamics were comparable to the DMET estimates, fluxes were highly different between various regions in the Rhine basin.

Results indicated that consistent parameter fields on various resolutions could be obtained with the used method. Modeled actual evapotranspiration fluxes remained preserved on coarser spatial resolutions, which is in agreement with the findings of Samaniego et al. (2010), Kumar, Samaniego, et al. (2013) and Samaniego et al. (2017). Recharge fluxes were only preserved for regions where the fluxes were considerably higher than 0. In the other regions, local relative errors of ±30% (sometimes up to 50%) occurred on a pixel to pixel scale. Catchment-averaged fluxes were, however, better preserved on the four resolutions.

Moreover, flux preservation was not found for routed discharge in smaller rivers and headwaters on coarser resolutions, while the routed discharge for the main course of the Rhine was consistent on all four resolutions. The headwaters rely most on well scaled slopes, river, and drainage networks. In areas where the network is dense and not well scaled to the model resolution, this leads to a river network and lateral subsurface flows that have slightly different directions and locations than on the highest resolution. For wflow_sbm, a model that allows for lateral subsurface flows, it requires a structural change in the model process of slope, river, and drainage network derivation from spatial information, such as the DEM. Ideally, this takes place on a subgrid scale in order to better represent the drainage processes on smaller scales. Research in this direction is currently underway.

Appendix A: Used Data Sets

Table A1 gives a list of the available and used data sets in this study. Some of these data sets are already briefly introduced in section 2.2.

Table A1
List of Available Data Sets in This Study

Name data set	Unit	Additional information	Source
Precipitation (genRE)	mm	Time period: 1996–2015	Van Osnabrugge et al. (2017)
Air temperature	°C	Time period: 1996–2015	Van Osnabrugge et al. (2019)
Potential evapotranspiration	mm	Time period: 1996–2015	Van Osnabrugge et al. (2019)
LSA SAF DMET (ET_{act}, 9 km^2)	mm	Time period: starting from 14 November 2011	Trigo et al. (2011)
Discharge at multiple locations in the Rhine basin	m^3 s^{-1}	Time period: 1997–2015	Same as used in Van Osnabrugge et al. (2017)
Leaf Area Index	m^2 m^{-2}	Time period: monthly 2000–2002 until 2017–2002	Myneni et al. (2015)
ISRIC SoilGrids 250m	—	See below	Hengl et al. (2017)
	kg m^{-3}	Bulk density	
	—	Soil types	
	kg m^{-3}	Soil organic carbon	
	%	Sand content	
	%	Clay content	
	%	Silt content	
	cm	Depth to bedrock	
ESDAC depth to impermeable layers	Classes (cm)		ESDAC (2004) and Panagos et al. (2012)
Global land cover	—		European Environment Agency (2018)

Appendix B: Used Pedotransfer Functions

PTFs consisting of equations are illustrated in Table B1. This table is an addition to Table 1 in section 3.1.2, and it briefly states the equations behind the PTFs. Lookup tables and more detailed descriptions of the PTFs are given in the supporting information.

Table B1
List of Parameters Estimated With a PTF Consisting of an (Empirical) Equation

Parameter	Equation[a]		Source
c			Rawls and Brakensiek (1989)
	$$c = 3 + \frac{2}{\lambda}$$	(B1)	
	$$\lambda = exp[-0.784 + 0.018 \cdot Sa - 1.062 \cdot \theta_s - Sa^2 \cdot (5 \cdot 10^{-5}) - 0.003 \cdot Cl^2$$		
	$$+ 1.111 \cdot \theta_s^2 - 0.031 \cdot Sa \cdot \theta_s + (3 \cdot 10^{-4}) \cdot Sa^2 \cdot \theta_s^2 - 0.006 \cdot Cl^2$$	(B2)	
	$$\cdot \theta_s^2 - (2 \cdot 10^{-6}) \cdot Sa^2 \cdot Cl + 0.008 \cdot Cl^2 \cdot \theta_s - 0.007 \cdot \theta_s^2 \cdot Cl]$$		
KsatVer			Brakensiek et al. (1984)
	$$K_s = 240.19 \cdot exp[19.52348 \cdot \theta_s - 8.96847 - 0.028212 \cdot Cl + (1.8107 \cdot 10^{-4})$$		
	$$\cdot Sa^2 - (9.4125 \cdot 10^{-3}) \cdot Cl^2 - 8.395215 \cdot \theta_s^2 + 0.077718 \cdot Sa \cdot \theta_s$$		
	$$- 0.00298 \cdot Sa^2 \cdot \theta_s^2 - 0.019492 \cdot Cl^2 \cdot \theta_s^2 + (1.73 \cdot 10^{-5}) \cdot Sa^2 \cdot Cl$$	(B3)	
	$$+ 0.02733 \cdot Cl^2 \cdot \theta_s + 0.001434 \cdot Sa^2 \cdot \theta_s - (3.5 \cdot 10^{-6}) \cdot Cl^2 \cdot Sa]$$		
M			
	$$K_s(z_i) = K_s(0) \cdot e^{-f \cdot z_i}$$	(B4)	
	$$f = \frac{\theta_s - \theta_r}{M}$$	(B5)	
θ_r & θ_s			Tóth et al. (2015)

Table B1 (continued)

Parameter	Equation[a]	Source
	$$\theta_r = 0.09878 + 0.002127 \cdot Cl - (8.366 \cdot 10^{-4}) \cdot Si - \frac{0.0767}{OC+1} + Si \cdot Cl$$ $$\cdot (3.853 \cdot 10^{-5}) + \frac{0.00233 \cdot Cl}{OC+1} + \frac{(9.498 \cdot 10^{-4}) \cdot Si}{OC+1}$$	(B6)
	$$\theta_s = 0.6819 + \frac{0.06480}{OC+1} - 0.119 \cdot BD^2 - 0.02668 + (8.031 \cdot 10^{-4}) \cdot Si + \frac{0.02321 \cdot BD^2}{OC+1}$$ $$+ Cl \cdot 0.001489 + 0.01908 \cdot BD^2 - 0.001109 \cdot Cl - (2.315 \cdot 10^{-5})$$ $$\cdot Si \cdot Cl - 0.001197 \cdot Si \cdot BD^2 - (1.068 \cdot 10^{-4}) \cdot Cl \cdot BD^2$$	(B7)

Note. Only the abbreviated parameter names are illustrated; see Table 2 for the interpretation of the parameters.

[a]Sa is % sand, Cl % clay, Si % silt, BD is the bulk density (g cm^{-3}), OC % organic carbon, OM % organic matter (approximated as $1.724 * OC$; Van Bemmelen, 1890).

References

Albergel, C., Balsamo, G., Rosnay, P. D., Munñoz-Sabater, J., & Boussetta, S. (2012). A bare ground evaporation revision in the ECMWF land-surface scheme: Evaluation of its impact using ground soil moisture and satellite microwave data. *Hydrology and Earth System Sciences*, *16*(10), 3607–3620. https://doi.org/10.5194/hess-16-3607-2012

Archfield, S. A., Clark, M. P., Arheimer, B., Hay, L. E., McMillan, H., Kiang, J. E., et al. (2015). Accelerating advances in continental domain hydrologic modeling. *Water Resources Research*, *12*, 10,078–10,091. https://doi.org/10.1002/2015WR017498

Balsamo, G., Beljaars, A., Scipal, K., Viterbo, P., van den Hurk, B., Hirschi, M., & Betts, A. K. (2009). A revised hydrology for the ECMWF model: Verification from field site to terrestrial water storage and impact in the Integrated Forecast System. *Journal of Hydrometeorology*, *10*(3), 623–643. https://doi.org/10.1175/2008JHM1068.1

Bell, V. A., Kay, A. L., Jones, R. G., & Moore, R. J. (2007). Development of a high resolution grid-based river flow model for use with regional climate model output. *Hydrology and Earth System Sciences Discussions*, *11*(1), 532–549. https://doi.org/10.5194/hess-11-532-2007

Benning, R. G. (1994). Towards a new lumped parameterization at catchment scale (Ph.D. Thesis), Wageningen, The Netherlands. http://edepot.wur.nl/216531ID

Beven, K. (1989). Changing ideas in hydrologythe case of physically-based models. *Journal of Hydrology*, *105*(1-2), 157–172. https://doi.org/10.1016/0022-1694(89)90101-7

Beven, K. (2006). Searching for the Holy Grail of scientific hydrology: Q_t=(S, R, Δt)A as closure. *Hydrology and Earth System Sciences*, *10*(5), 609–618. https://doi.org/10.5194/hess-10-609-2006

Bierkens, M. F. P. (2015). Global hydrology 2015: State, trends, and directions. *Water Resources Research*, *51*, 4923–4947. https://doi.org/10.1002/2015WR017173

Bierkens, M. F. P., & Van Beek, L. P. H. (2009). Seasonal predictability of European discharge: NAO and hydrological response time. *Journal of Hydrometeorology*, *10*(4), 953–968. https://doi.org/10.1175/2009JHM1034.1

Blöschl, G., & Sivapalan, M. (1995). Scale issues in hydrological modelling: A review. *Hydrological Processes*, *9*(3-4), 251–290. https://doi.org/10.1002/hyp.3360090305

Brakensiek, D. L., Rawls, W. J., & Stephenson, G. R. (1984). Modifying SCS hydrologic soil groups and curve numbers for rangeland soils. American Society of Agricultural Engineers, PNR-84-203.

Brooks, R., & Corey, T. (1964). Hydraulic properties of porous media. *Hydrology Papers, Colorado State University*, *7*, 26–28. https://doi.org/10.13031/2013.40684

Clark, M. P., Bierkens, M. F. P., Samaniego, L., Woods, R. A., Uijlenhoet, R., Bennett, K. E., et al. (2017). The evolution of process-based hydrologic models: Historical challenges and the collective quest for physical realism. *Hydrology and Earth System Sciences*, *21*(7), 3427–3440. https://doi.org/10.5194/hess-21-3427-2017

Clark, M. P., Schaefli, B., Schymanski, S. J., Samaniego, L., Luce, C. H., Jackson, B. M., et al. (2016). Improving the theoretical underpinnings of process-based hydrologic models. *Water Resources Research*, *52*, 2350–2365. https://doi.org/10.1002/2015WR017910

De Bruin, H. A. R., Trigo, I. F., Bosveld, F. C., & Meirink, J. F. (2016). A thermodynamically based model for actual evapotranspiration of an extensive grass field close to FAO reference, suitable for remote sensing application. *Journal of Hydrometeorology*, *17*(5), 1373–1382. https://doi.org/10.1175/JHM-D-15-0006.1

Demirel, M. C., Mai, J., Mendiguren, G., Koch, J., Samaniego, L., & Stisen, S. (2018). Combining satellite data and appropriate objective functions for improved spatial pattern performance of a distributed hydrologic model. *Hydrology and Earth System Sciences*, *22*(2), 1299–1315. https://doi.org/10.5194/hess-22-1299-2018

Dorigo, W. A., Wagner, W., Albergel, C., Albrecht, F., Balsamo, G., Brocca, L., et al. (2017). ESA CCI soil moisture for improved Earth system understanding: State-of-the art and future directions. *Remote Sensing of Environment*, *203*, 185–215. https://doi.org/10.1016/j.rse.2017.07.001

Dunn, S. M., & Colohan, R. J. E. (1999). Developing the snow component of a distributed hydrological model: A step-wise approach based on multiobjective analysis. *Journal of Hydrology*, *223*(1-2), 1–16. https://doi.org/10.1016/S0022-1694(99)00095-5

ESDAC (2004). The European Soil Database distribution version 2.0, European Commission and the European Soil Bureau Network. Retrieved from esdac.jrc.ec.europa.eu

Engman, E. (1986). Roughness coefficients for routing surface runoff. *Journal of Irrigation and Drainage Engineering*, *112*(1), 39–53. https://doi.org/10.1061/(ASCE)0733-9437(1986)112:1(39)

European Environment Agency (2018). Corine Land Cover (CLC) 2018, Version 20. Retrieved from https://land.copernicus.eu/pan-european/corine-land-cover/clc2018?tab=metadata

Fan, J., McConkey, B., Wang, H., & Janzen, H. (2016). Root distribution by depth for temperate agricultural crops. *Field Crops Research*, *189*, 68–74. https://doi.org/10.1016/j.fcr.2016.02.013

Farr, T. G., Rosen, P. A., Caro, E., Crippen, R., Duren, R., Hensley, S., et al. (2007). The shuttle radar topography mission. *Reviews of Geophysics*, *45*, RG2004. https://doi.org/10.1029/2005RG000183

Fatichi, S., Vivoni, E. R., Ogden, F. L., Ivanov, V. Y., Mirus, B., Gochis, D., et al. (2016). An overview of current applications, challenges, and future trends in distributed process-based models in hydrology. *Journal of Hydrology*, *537*, 45–60. https://doi.org/10.1016/j.jhydrol.2016.03.026

Feddes, R. A., Kowalik, P. J., & Zaradny, H. (1978). Water uptake by plant roots. In R. A. Feddes, P. J. Kowalik, & H. Zaradny (Eds.), *Simulation of field water use and crop yield* (pp. 16–30). New York, NY: John Wiley & Sons, Inc.

Ficchì, A., Perrin, C., & Andréassian, V. (2019). Hydrological modelling at multiple sub-daily time steps: Model improvement via flux-matching. *Journal of Hydrology*, *575*, 1308–1327. https://doi.org/10.1016/j.jhydrol.2019.05.084

Fischer, M., Huss, M., Barboux, C., & Hoelzle, M. (2014). The new Swiss Glacier Inventory SGI2010: Relevance of using high-resolution source data in areas dominated by very small glaciers. *Arctic, Antarctic, and Alpine Research*, *46*(4), 933–945. https://doi.org/10.1657/1938-4246-46.4.933

Görgen, K., Beersma, J., Brahmer, G., Buiteveld, H., Carambia, M., de Keizer, O., et al. (2010). *Assessment of climate change impacts on discharge in the Rhine River Basin: Results of the RheinBlick2050 project*. Lelystad, Netherlands: Internationale Kommission für die Hydrologie des Rheingebietes.

Gash, J. H. C. (1979). An analytical model of rainfall interception by forests. *Quarterly Journal of the Royal Meteorological Society*, *105*(443), 43–55. https://doi.org/10.1002/qj.49710544304

Grinsted, A. (2013). An estimate of global glacier volume. *The Cryosphere*, *7*(1), 141–151. https://doi.org/10.5194/tc-7-141-2013

Gupta, H. V., Kling, H., Yilmaz, K. K., & Martinez, G. F. (2009). Decomposition of the mean squared error and NSE performance criteria: Implications for improving hydrological modelling. *Journal of Hydrology*, *377*(1), 80–91. https://doi.org/10.1016/j.jhydrol.2009.08.003

Hengl, T., de Jesus, J. M., Heuvelink, G. B. M., Gonzalez, M. R., Kilibarda, M., Blagotić, A., et al. (2017). SoilGrids250m: Global gridded soil information based on machine learning. *PloS one*, *12*(2), e0169748. https://doi.org/10.1371/journal.pone.0169748

Hock, R. (2003). Temperature index melt modelling in mountain areas. *Journal of Hydrology*, *282*(1-4), 104–115. https://doi.org/10.1016/S0022-1694(03)00257-9

Hurkmans, R. T. W. L., de Moel, H., Aerts, J. C. J. H., & Troch, P. A. (2008). Water balance versus land surface model in the simulation of Rhine river discharges. *Water Resources Research*, *44*, W01418. https://doi.org/10.1029/2007WR006168

Hurkmans, R. T. W. L., Terink, W., Uijlenhoet, R., Moors, E. J., Troch, P. A., & Verburg, P. H. (2009). Effects of land use changes on stream flow generation in the Rhine basin. *Water Resources Research*, *45*, W06405. https://doi.org/10.1029/2008WR007574

Hurkmans, R. T. W. L., Terink, W., Uijlenhoet, R., Torfs, P., Jacob, D., & Troch, P. A. (2010). Changes in streamflow dynamics in the Rhine basin under three high-resolution regional climate scenarios. *Journal of Climate*, *23*(3), 679–699. https://doi.org/10.1175/2009JCLI3066.1

Jörg-Hess, S., Fundel, F., Jonas, T., & Zappa, M. (2014). Homogenisation of a gridded snow water equivalent climatology for Alpine terrain: Methodology and applications. *The Cryosphere*, *8*(2), 471–485. https://doi.org/10.5194/tc-8-471-2014

Karssenberg, D., Schmitz, O., Salamon, P., de Jong, K., & Bierkens, M. F. P. (2010). A software framework for construction of process-based stochastic spatio-temporal models and data assimilation. *Environmental Modelling & Software*, *25*(4), 489–502. https://doi.org/10.1016/j.envsoft.2009.10.004

Kilgore, J. L. (1997). Development and evaluation of a GIS-based spatially distributed unit hydrograph model (MSc thesis). Retrieved from http://hdl.handle.net/10919/35777

Koch, J., Demirel, M. C., & Stisen, S. (2018). The SPAtial EFficiency metric (SPAEF): Multiple-component evaluation of spatial patterns for optimization of hydrological models. *Geoscientific Model Development*, *11*(5), 1873–1886.

Krysanova, V., Vetter, T., Eisner, S., Huang, S., Pechlivanidis, I., Strauch, M., et al. (2017). Intercomparison of regional-scale hydrological models and climate change impacts projected for 12 large river basins worldwide synthesis. *Environmental Research Letters*, *12*(10), 105,002. https://doi.org/10.1088/1748-9326/aa8359

Kumar, R., Livneh, B., & Samaniego, L. (2013). Toward computationally efficient large-scale hydrologic predictions with a multiscale regionalization scheme. *Water Resources Research*, *49*, 5700–5714. https://doi.org/10.1002/wrcr.20431

Kumar, R., Samaniego, L., & Attinger, S. (2013). Implications of distributed hydrologic model parameterization on water fluxes at multiple scales and locations. *Water Resources Research*, *49*, 360–379. https://doi.org/10.1029/2012WR012195

Kunnath-Poovakka, A., Ryu, D., Renzullo, L., & George, B. (2016). The efficacy of calibrating hydrologic model using remotely sensed evapotranspiration and soil moisture for stream flow prediction. *Journal of Hydrology*, *535*, 509–524. https://doi.org/10.1016/j.jhydrol.2016.02.018

Kuusisto, E. (1984). *Snow accumulation and snowmelt in Finland*. Finland: Vesihallitus, National Board of Waters.

Lindström, G., Johansson, B., Persson, M., Gardelin, M., & Bergström, S. (1997). Development and test of the distributed HBV-96 hydrological model. *Journal of Hydrology*, *201*(1-4), 272–288. https://doi.org/10.1016/S0022-1694(97)00041-3

Liu, S. (1998). Estimation of rainfall storage capacity in the canopies of cypress wet lands and slash pine uplands in North-Central Florida. *Journal of Hydrology*, *207*(1-2), 32–41. https://doi.org/10.1016/S0022-1694(98)00115-2

Liu, Z., Martina, M. L. V., & Todini, E. (2005). Flood forecasting using a fully distributed model: Application of the TOPKAPI model to the Upper Xixian Catchment. *Hydrology and Earth System Sciences Discussions*, *9*(4), 347–364. https://doi.org/10.5194/hess-9-347-2005

Luo, Y., Arnold, J., Liu, S., Wang, X., & Chen, X. (2013). Inclusion of glacier processes for distributed hydrological modeling at basin scale with application to a watershed in Tianshan Mountains, northwest China. *Journal of Hydrology*, *477*, 72–85. https://doi.org/10.1016/j.jhydrol.2012.11.005

Melsen, L. A., Teuling, A. J., Torfs, P. J. J. F., & Clark, M. P. (2016). HESS opinions: The need for process-based evaluation of large-domain hyper resolution models. *Hydrology and Earth System Sciences*, *20*(3), 1069–1079. https://doi.org/10.5194/hess-20-1069-2016

Middelkoop, H., Daamen, K., Gellens, D., Grabs, W., Kwadijk, J. C. J., Lang, H., et al. (2001). Impact of climate change on hydrological regimes and water resources management in the Rhine basin. *Climatic Change*, *49*(1), 105–128. https://doi.org/10.1023/A:1010784727448

Mizukami, N., Clark, M. P., Newman, A. J., Wood, A. W., Gutmann, E. D., Nijssen, B., et al. (2017). Towards seamless large-domain parameter estimation for hydrologic models. *Water Resources Research*, *53*, 8020–8040. https://doi.org/10.1002/2017WR020401

Myneni, R. B., Knyazikhin, Y., & Park, T. (2015). MCD15A3H MODIS/Terra+Aqua Leaf Area Index/FPAR 4-day L4 Global 500m SIN Grid V006 (*Tech. Rep.*): NASA EOSDIS and Pocesses DAAC.

Nash, J. E., & Sutcliffe, J. V. (1970). River flow forecasting through conceptual models part IA discussion of principles. *Journal of Hydrology*, *10*(3), 282–290. https://doi.org/10.1016/0022-1694(70)90255-6

Nijzink, R. C., Samaniego, L., Mai, J., Kumar, R., Thober, S., Zink, M., et al. (2016). The importance of topography-controlled sub-grid process heterogeneity and semi-quantitative prior constraints in distributed hydrological models. *Hydrology and Earth System Sciences*, *20*(3), 1151–1176. https://doi.org/10.5194/hess-20-1151-2016

Niu, G.-Y., Yang, Z.-L., Mitchell, K. E., Chen, F., Ek, M. B., Barlage, M., et al. (2011). The community Noah land surface model with multiparameterization options (Noah-MP): 1. Model description and evaluation with local-scale measurements. *Journal of Geophysical Research*, *116*, D12110. https://doi.org/10.1029/2010JD015140

Panagos, P., Van Liedekerke, M., Jones, A., & Montanarella, L. (2012). European soil data centre: Response to European policy support and public data requirements. *Land Use Policy*, *29*(2), 329–338. https://doi.org/10.1016/j.landusepol.2011.07.003

Paniconi, C., & Putti, M. (2015). Physically based modeling in catchment hydrology at 50: Survey and outlook. *Water Resources Research*, *51*, 7090–7129.

Photiadou, C. S., Weerts, A. H., & Van den Hurk, B. J. J. M. (2011). Evaluation of two precipitation data sets for the Rhine River using streamflow simulations. *Hydrology and Earth System Sciences*, *15*(11), 3355–3366. https://doi.org/10.5194/hess-15-3355-2011

Pitman, J. (1989). Rainfall interception by bracken in open habitats—Relations between leaf area, canopy storage and drainage rate. *Journal of Hydrology*, *105*(3-4), 317–334. https://doi.org/10.1016/0022-1694(89)90111-X

RGI Consortium (2017). Randolph glacier inventory—A dataset of global glacier outlines: Version 6.0 (*Tech. Rep.*) CO, USA: Global Land Ice Measurements from Space.

Rakovec, O., Kumar, R., Attinger, S., & Samaniego, L. (2016). Improving the realism of hydrologic model functioning through multivariate parameter estimation. *Water Resources Research*, *52*, 7779–7792. https://doi.org/10.1002/2016WR019430

Rakovec, O., Kumar, R., Mai, J., Cuntz, M., Thober, S., Zink, M., et al. (2016). Multiscale and multivariate evaluation of water fluxes and states over European river basins. *Journal of Hydrometeorology*, *17*(1), 287–307. https://doi.org/10.1175/JHM-D-15-0054.1

Raup, B. H., Racoviteanu, A., Khalsa, S. J. S., Helm, C., Armstrong, R., & Arnaud, Y. (2007). The GLIMS geospatial glacier database: A new tool for studying glacier change. *Global and Planetary Change*, *56*, 101–110. https://doi.org/10.1016/j.gloplacha.2006.07.018

Rawls, W. J., & Brakensiek, D. L. (1989). Estimation of soil water retention and hydraulic properties. In H. J. Morel-Seytoux (Ed.), *Unsaturated flow in hydrologic modelling—Theory and practice* (pp. 275–300). Dordrecht, The Netherlands: Kluwer Academic Publishing. https://doi.org/10.1007/978-94-009-2352-2_10

Reggiani, P., & Weerts, A. H. (2008). A Bayesian approach to decision-making under uncertainty: An application to real-time forecasting in the river Rhine. *Journal of Hydrology*, *356*(1-2), 56–69. https://doi.org/10.1016/j.jhydrol.2008.03.027

Renner, M., Werner, M. G. F., Rademacher, S., & Sprokkereef, E. (2009). Verification of ensemble flow forecasts for the River Rhine. *Journal of Hydrology*, *376*(3-4), 463–475. https://doi.org/10.1016/j.jhydrol.2009.07.059

Rutter, A. J., Kershaw, K. A., Robins, P. C., & Morton, A. J. (1971). A predictive model of rainfall interception in forests, 1. Derivation of the model from observations in a plantation of Corsican pine. *Agricultural Meteorology*, *9*, 367–384. https://doi.org/10.1016/0002-1571(71)90034-3

Rutter, A. J., Morton, A. J., & Robins, P. C. (1975). A predictive model of rainfall interception in forests. II. Generalization of the model and comparison with observations in some coniferous and hardwood stands. *Journal of Applied Ecology*, *17*, 367–380. https://doi.org/10.2307/2401739

Samaniego, L., Kumar, R., & Attinger, S. (2010). Multiscale parameter regionalization of a grid-based hydrologic model at the mesoscale. *Water Resources Research*, *46*, W05523. https://doi.org/10.1029/2008WR007327

Samaniego, L., Kumar, R., Thober, S., Rakovec, O., Zink, M., Wanders, N., et al. (2017). Toward seamless hydrologic predictions across spatial scales. *Hydrology and Earth System Sciences*, *21*(9), 4323–4346. https://doi.org/10.5194/hess-21-4323-2017

Schellekens, J., Van Verseveld, W., Visser, M., Winsemius, H., Euser, T., Bouaziz, L., et al. (2020). Openstreams/wflow: Unstable-master. https://github.com/openstreams/wflow

Schenk, H. J., & Jackson, R. B. (2002). The global biogeography of roots. *Ecological Monographs*, *72*(3), 311–328. https://doi.org/10.1890/0012-9615(2002)072[0311:TGBOR]2.0.CO;2

Seibert, J. (1999). Regionalisation of parameters for a conceptual rainfall-runoff model. *Agricultural and Forest Meteorology*, *98*, 279–293. https://doi.org/10.1016/S0168-1923(99)00105-7

Semádeni-Davies, A. (1997). Monthly snowmelt modelling for large-scale climate change studies using the degree day approach. *Ecological Modelling*, *101*(2-3), 303–323. https://doi.org/10.1016/S0304-3800(97)00054-9

Sivapalan, M., Blöschl, G., Zhang, L., & Vertessy, R. (2003). Downward approach to hydrological prediction. *Hydrological Processes*, *17*(11), 2101–2111.

Stisen, S., McCabe, M., Refsgaard, J., Lerer, S., & Butts, M. (2011). Model parameter analysis using remotely sensed pattern information in a multiconstraint framework. *Journal of Hydrology*, *409*(1), 337–349. https://doi.org/10.1016/j.jhydrol.2011.08.030

Te Linde, A. H., Aerts, J. C. J. H., Bakker, A. M. R., & Kwadijk, J. C. J. (2010). Simulating low-probability peak discharges for the Rhine basin using resampled climate modeling data. *Water Resources Research*, *46*, W03512. https://doi.org/10.1029/2009WR007707

Thober, S., Cuntz, M., Kelbling, M., Kumar, R., Mai, J., & Samaniego, L. (2019). The multiscale routing model mRM v1.0: Simple river routing at resolutions from 1 to 50 km. *Geoscientific Model Development*, *12*(6), 2501–2521. https://doi.org/10.5194/gmd-12-2501-2019

Tobin, C., Schaefli, B., Nicótina, L., Simoni, S., Barrenetxea, G., Smith, R., et al. (2013). Improving the degree-day method for sub-daily melt simulations with physically-based diurnal variations. *Advances in Water Resources*, *55*, 149–164. https://doi.org/10.1016/j.advwatres.2012.08.008

Todini, E., & Ciarapica, L. (2002). The TOPKAPI model. In V. P. Singh, & D. K. Frevert (Eds.), *Mathematical models of large watershed hydrology* (pp. 471–506). Littleton, CO: Water Resources Publications.

Tóth, B., Weynants, M., Nemes, A., Makó, A., Bilas, G., & Tóth, G. (2015). New generation of hydraulic pedotransfer functions for Europe. *European Journal of Soil Science*, *66*, 226–238. https://doi.org/10.1111/ejss.12192

Trigo, I. F., Dacamara, C. C., Viterbo, P., Roujean, J.-L., Olesen, F., Barroso, C., et al. (2011). The satellite application facility for land surface analysis. *International Journal of Remote Sensing*, *32*(10), 2725–2744. https://doi.org/10.1080/01431161003743199

Van Beek, L. P. H., Wada, Y., & Bierkens, M. F. P. (2011). Global monthly water stress: 1. Water balance and water availability. *Water Resources Research*, *47*, W07518. https://doi.org/10.1029/2010WR009792

Van Bemmelen, J. M. (1890). Über die Bestimmung des Wassers, des Humus, des Schwefels, der in den colloïdalen Silikaten gebundenen Kieselsäure, des Mangans u. s. w. im Ackerboden. *Die Landwirthschaftlichen Versuchs-Stationen*, *37*, 279–290.

Van Den Hurk, B. J. J. M., Bouwer, L. M., Buontempo, C., Döscher, R., Ercin, E., Hananel, C., et al. (2016). Improving predictions and management of hydrological extremes through climate services: www.imprex.eu. *Climate Services*, *1*, 6–11. https://doi.org/10.1016/j.cliser.2016.01.001

Van Dijk, A. I. J. M., & Bruijnzeel, L. A. (2001). Modelling rainfall interception by vegetation of variable density using an adapted analytical model. Part 2. Model validation for a tropical upland mixed cropping system. *Journal of Hydrology*, *247*(3-4), 239–262.

Van Griensven, A., Meixner, T., Grunwald, S., Bishop, T., Diluzio, M., & Srinivasan, R. (2006). A global sensitivity analysis tool for the parameters of multi-variable catchment models. *Journal of Hydrology*, *324*(1), 10–23. https://doi.org/10.1016/j.jhydrol.2005.09.008

Van Looy, K., Bouma, J., Herbst, M., Koestel, J., Minasny, B., Mishra, U., et al. (2017). Pedotransfer functions in Earth system science: Challenges and perspectives. *Reviews of Geophysics*, *55*, 1199–1256. https://doi.org/10.1002/2017RG000581

Van Osnabrugge, B., Uijlenhoet, R., & Weerts, A. H. (2019). Contribution of potential evaporation forecasts to 10-day streamflow forecast skill for the Rhine River. *Hydrology and Earth System Sciences*, *23*(3), 1453–1467. https://doi.org/10.5194/hess-23-1453-2019

Van Osnabrugge, B., Weerts, A. H., & Uijlenhoet, R. (2017). genRE: A method to extend gridded precipitation climatology data sets in near real-time for hydrological forecasting purposes. *Water Resources Research*, *53*, 9284–9303. https://doi.org/10.1002/2017WR021201

Van den Hurk, B. J. J. M., Viterbo, P., Beljaars, A. C. M., & Betts, A. K. (2000). Offline validation of the ERA40 surface scheme, *ECMWF Technical Memoranda*. Reading, United Kingdom: European Centre for Medium-Range Weather Forecasts. https://doi.org/10.21957/9aoaspz8

Verkade, J. S., Brown, J. D., Davids, F., Reggiani, P., & Weerts, A. H. (2017). Estimating predictive hydrological uncertainty by dressing deterministic and ensemble forecasts: A comparison, with application to Meuse and Rhine. *Journal of Hydrology*, *555*, 257–277. https://doi.org/10.1016/j.jhydrol.2017.10.024

Vertessy, R. A., & Elsenbeer, H. (1999). Distributed modeling of storm flow generation in an Amazonian rain forest catchment: Effects of model parameterization. *Water Resources Research*, *35*(7), 2173–2187. https://doi.org/10.1029/1999WR900051

Viterbo, P., & Beljaars, A. C. M. (1995). An improved land surface parameterization scheme in the ECMWF model and its validation. *Journal of Climate*, *8*(11), 2716–2748. https://doi.org/10.1175/1520-0442(1995)008<2716:AILSPS>2.0.CO;2

Wanders, N., Bierkens, M. F. P., de Jong, S. M., de Roo, A., & Karssenberg, D. (2014). The benefits of using remotely sensed soil moisture in parameter identification of large-scale hydrological models. *Water Resources Research*, *50*, 6874–6891. https://doi.org/10.1002/2013WR014639

Wit, M. J. M., & Buishand, T. A. (2007). Generator of rainfall and discharge extremes (GRADE) for the Rhine and Meuse basins.

Zhu, J., & Mohanty, B. P. (2002). Spatial averaging of van Genuchten hydraulic parameters for steady-state flow in heterogeneous soils. *Vadose Zone Journal*, *2*(1), 261–272. https://doi.org/10.2136/vzj2002.2610